CLASSIFICATION OF AEROSOLS AND DETERMINATION OF MINERAL DUST TRANSPORT PATHS TO EASTERN MEDITERRANEAN REGIONS OF TURKEY

AEROSOLLERIN SINIFLANDIRILMASI VE TÜRKİYE'NİN DOĞU AKDENİZ BÖLGELERİNE MİNERAL TOZU TAŞIMA YOLLARININ BELİRLENMESİ

GÜLŞAH AKGÜL

PROF. DR GÜLEN GÜLLÜ

Supervisor

Submitted to

Graduate School of Science and Engineering of Hacettepe University

as a Partial Fulfillment to the Requirements

for the Award of the Degree of Master of Science

in Environmental Engineering.

January 2023

ABSTRACT

CLASSIFICATION OF AEROSOLS AND DETERMINATION OF MINERAL DUST TRANSPORT PATHS TO EASTERN MEDITERRANEAN REGIONS OF TURKEY

Gülşah AKGÜL

Master of Science, Department of Environmental Engineering

Supervisor: Prof. Dr. Gülen Güllü

January 2023, 61 pages

Atmospheric aerosols are liquid and solid particles dispersed in a gas. Aerosols are emitted into the atmosphere through anthropogenic sources or natural sources. They cause adverse effects on human health. Additionally, they can scatter and absorb light from the sun. While they reduce the amount of sunlight reaching the atmosphere with their scattering properties, they increase the amount of radiation retained in the atmosphere with their absorption properties. Most of them scatter solar radiation, while some absorb it. Its net effects are known to cause cooling in the atmosphere. They should be classified according to their source, size, and chemical structure to evaluate their impacts. Dust is one of the most common aerosols of natural origin in the atmosphere. It is thought that dust transport from the deserts in the south of Turkey, especially to the southern regions, occurs and increases the aerosol load. This study classified aerosols in the region according to their optical properties. As a result of the classification, aerosols released from combustion, industrial aerosols, newly formed smoke aerosols, and dust aerosols were found in the region. It was determined that the aerosol load in the region increased with dust transport, and the highest increase was observed in the spring, while the lowest increase was observed in the winter. The rough mode volume density ratio representing dust to the total amount of aerosol is 95-99% for spring and 90-93% for other seasons when the dust is transported. As a result of the wind analysis, it was determined that the region received wind from the deserts located in the south.

Keywords: Aerosol Classification, Dust, Dust Transport, Eastern Mediterranean

ÖZET

AEROSOLLERIN SINIFLANDIRILMASI VE TÜRKİYE'NİN DOĞU AKDENİZ BÖLGELERİNE MİNERAL TOZU TAŞIMA YOLLARININ BELİRLENMESİ

Gülşah AKGÜL

Yüksek Lisans, Çevre Mühendisliği Bölümü

Tez Danışmanı: Prof. Dr. Gülen Güllü

Ocak 2023, 61 sayfa

Atmosferik aerosoller, bir gaz içinde dağılmış sıvı ve katı parçacıklardır. Aerosoller antropojenik kaynaklar veya doğal kaynaklar yoluyla atmosfere yayılırlar.insan sağlığı üzerinde olumsuz etkilere sebep olmakla birlikte güneşten gelen ışığı yansıtma ve absorbe etme özellikleri bulunmaktadır. Yansıtma özellikleri ile atmosfere ulaşan güneş ışığı miktarını azaltırken absorbe etme özellikleri ile atmosferde tutulan radyosyan miktarını artırmaktadırlar. Büyük bir bölümleri güneş radyasyonunu yansıtırken bir kısmı ise absorbe etmektedir. Net etkilerinin atmosferde soğumaya neden olduğu bilinmektedir. Bir bölgede ortaya çıkan etkilerinin değerlendirilmesi için kaynaklarına, boyutlarına ve kimyasal yapılarına göre sınıflandırılmaları gerekmektedir. Doğal kaynaklı aerosollerden atmosferde en çok rastalanan türlerden birisi tozdur. Türkiye'nin güneyinde yer alan çöllerden özellikle güney bölgelerine toz taşınımı meydana geldiği ve aerosol yükünü artırdığı düşünülmektedir. Bu çalışma, bölgedeki aerosolleri optik özelliklerine göre sınıflandırmıştır. Yapılan sınıflandırma sonucunda bölgede yanma sonucu açığa çıkan aerosoller, endüstri kaynaklı aerosoller, yeni oluşmuş duman aerosolleri ile birlikte toz aerosollerine rastlanmıştır. Tüm yıl boyunca bölgede aerosol yükünün toz taşınımı ile arttığı belirlenmiş ve en yüksek artış ilkbaharda görülürken en düşük artış kışta görülmüştür. Toz taşınımı olduğu zamanlarda tozu temsil eden kaba mod hacim yoğunluğunun toplam aerosol miktarına oranı ilkbahar için %95-99, diğer mevsimler için %90-93'tür. Yapılan rüzgar analizleri sonucunda bölgenin güneyde yer alan çöllerden rüzgar aldığı tespit edilmiştir.

Anahtar Kelimeler: Aerosol Sınıflandırma, Toz, Toz Taşınımı, Doğu Akdeniz

TABLE OF CONTENTS

LIST OF FIGURES

LIST OF TABLES

ICONS AND ABBREVIATIONS

Icons

α	Angstrom Exponent
β	Angstrom Turbidity Coefficient
C_i	Particle Volume Concentration
ε_{abs}	Absorption Coefficient
ε_{ext}	Extinction Coefficient
ε_{sct}	Scattering Coefficient
σ	Variance
λ	Wavelength
m	Refractive Index
N	Number Density
r	radius
τ	Aerosol Optical Thickness
Q_{ext}	Extinction coefficient
T	Transmission from molecular scattering

Abbreviations

AE	Angstrom Exponent
Á	Angstrom Exponent Difference
AERONET	Aerosol Robotic Network
agl	above ground level
AOT	Aerosol Optical Thickness
ARL	Air Sources Laboratory
BC	Black Carbon

BS	Black Smoke
CNN	Cloud Condensation Nuclei
CH_4	Methane
CO	Carbon Monoxide
CO_2	Carbon Dioxide
GDAS	Global Data Assimilation System
HYSPLIT_4	Hybrid Single-Particle Lagrangian Integrated Trajectory Version-4
IMS-METU-ERDEMLI	Erdemli
LIDAR	Laser Imaging Detection and Ranging
MSL	mean sea level
NOAA	US National Oceanic and Atmospheric Administration
NO_2	Nitrogen Dioxide
O_3	Ozone
OC	Organic Carbon
PBL	Planetary Boundary Layer
PM_{10}	Particulate Matter less than 10 μm in diameter
SSA	Single Scattering Albedo
SO_2	Sulfur Dioxide
VOCs	Volatile Organic Compounds
US	United States

1. INTRODUCTION

Atmospheric aerosols are liquid and solid particles dispersed in a gas. They are released through anthropogenic sources or natural sources. Anthropogenic sources of aerosols are the combustion of fossil fuels, industrial activities, transportation activities, fugitive emissions of industrial processes, construction and demolition activities, and cooking and heating activities from houses (Calvo et al., 2013). Natural sources of aerosols are mineral dust, sea salt, soil and rock debris, forest fire, and biogenic particles. Additionally, volcanic eruptions and vegetation gases are sources of naturally formed aerosols (Rap et al., 2013). The estimated global aerosol emissions are given in Table 1.1. Most aerosols are formed by natural sources and constitute nine-tenth of the total. Sea salt and dust aerosols are approximately half of the atmospheric aerosols. Anthropogenic aerosols constitute about 10 percent of the total.

Table 1.1. Emissions of main aerosol types (Andrews, 2010)

AEROSOL TYPE	**EMISSION (10^6 tons per year)**
Sea-salt	500-2000
From a gaseous phase	345-2080
Dust	7-1800
Biological	80
Smoke (forest fires)	5-150
Volcanic	4-90
Anthropogenic	181-396

The formation of aerosols relies on atmospheric and physical-chemical processes. They are emitted directly into the atmosphere or form from precursor gases and particles or through physical and chemical interactions. Aerosols have different physical and chemical properties according to their formation mechanism and chemical structure. Aerosols affect the heat budget of the atmosphere because they can absorb and scatter the incoming sunlight. While most of them scatter light, there are also light-absorbing types. Light-scattering aerosols have a general cooling effect in the atmosphere; conversely,

light-absorbing aerosols that trap the light cause warming. Considering their net effects, they cause cooling in the atmosphere. Moreover, they play an important role in cloud formation mechanisms and increase scattered light, indirectly affecting the heat budget. Apart from the heat balance effects on the atmosphere, there are adverse health effects on living things. They cause respiratory and heart diseases and allergy problems in humans.

Aerosols are classified based on chemical and physical properties. Physical properties of aerosols can be listed as number, shape, and size based on diameter, surface area, mass, size, and electrical charge distribution. The most common classifications by physical properties are size and optical properties. Atmospheric aerosol distributions are characterized according to size as nuclei or fine mode, accumulation mode, and coarse mode. According to optical properties, the most straightforward classification is absorbing and scattering aerosols.

Aerosol optical thickness (AOT) is the most widely used parameter for categorizing the optical properties of aerosols. AOT represents the degree of the prevented light transmission in a columnar due to total extinction (absorption and scattering). AOT measurements identify aerosols' optical properties, size distribution, and mass concentration. Angstrom Exponent (AE) is another important parameter of optical properties that represents AOT's wavelength dependence. AE has valuable information about particle size distribution; in general terms, AE <1 is related to coarse-mode aerosols, and AE >1 is related to fine-mode aerosols (Kaufman (1993)).

Three methods are used to obtain AOT and AE observations: ground base, space observations, and gridded data (Verma et al., 2019). Space observations are based on satellite remote sensing, which is the measurement by a recording device not in physical or close contact with the object under investigation. In satellite remote sensing, electromagnetic radiation is detected after interaction with the atmospheric components (Payan et al., 2005). Ground-based instruments measure solar radiation directly from the entire sky or the sun. A sun photometer is a ground-based instrument that measures solar radiation directly from the sun at various wavelengths. NASA created a network called AERONET (AErosol RObotic NETwork) of measurement results from sun photometers in different parts of the world. In Turkey, there are three AERONET stations; TUBITAK_UZAY_Ankara, and IMS-METU-ERDEMLI. While there are 14 years of data for the IMS-METU-ERDEMLI station, the measurements for the other two stations

were at most one year. In this study, the IMS-METU-ERDEMLI station will be called the Erdemli station.

Classification of natural aerosol gains importance because most aerosols are natural, and the effects of human-induced ones still need to be fully known (Andrews, 2010). Different aerosols have different physical properties and, accordingly, different effects. For example, aerosols of different sizes have different effects on health. small aerosols can enter the blood stream and affect different organs (Pöschl, 2005). Larger ones can cause health problems such as allergies (Mauderly & Chow, 2008). It is also known that they have different effects on the atmosphere. Although their net effect is to cool the atmosphere, some species absorb light and cause warming. Among the absorbing aerosols, the most famous are Black Carbon (BC), soot, and dust. Apart from its global effect, if the absorbing species are in the majority in a region, they can cause warming in that area. Dust aerosols tend to be larger than most aerosols and significantly increase the aerosol load.

This thesis aims to classify aerosols for the eastern Mediterranean region of Turkey using their physical properties, such as size and optical properties, and decide whether there is dust transport to the region. In the presence of dust transport, the effect of the aerosol load in the region and the transport routes are determined to show the importance of dust transport on the region's air quality. In this study, aerosol classification of the Eastern Mediterranean regions of Turkey has been done according to the seasons and months, and dust transport routes have been determined. In the following sections of the thesis, detailed information about the methods and data used for classification are given, and the results are discussed in Chapter 4.

2. LITERATURE REVIEW

2.1. Aerosols

Atmospheric aerosols are defined as liquid and solid particles dispersed in a gas. They formed through anthropogenic and natural sources. Anthropogenic sources of aerosols are the combustion of fossil fuels, industrial activities and their fugitive emissions, transportation activities, construction and demolition activities, and cooking and heating activities of houses (Calvo et al., 2013). The most important anthropogenic aerosol source is industrial activities. There is a wide variety of industrial activities, and the gases and particles released vary according to process and raw material. In mining activities and coal combustion, particle matter is released. Also, particle matter is released by industrial activities such as cement production. Additionally, trace elements are emitted from industrial and mining activities. Fossil fuel combustion produces a high amount of precursor gases (Calvo et al., 2013).

In urbanized areas, road traffic-originated aerosols released from vehicles' exhaust are one of the main anthropogenic aerosols; however, air and marine traffic also generate precursor gases and particles. Additionally, brake wear in vehicles can cause to release of particles with a significant amount of trace elements. Out of exhaust emissions, in non-paved roads, dust particles can enter the atmosphere due to vehicle activities. Traffic emissions are also the most important contributor to nitrogen oxide concentration in urbanized areas. Nitrogen oxide is known as a precursor gas that results in nitrate aerosols. Burning from human activities is classified as an anthropogenic source, and natural fires are a natural source of aerosols.

Biomass-burning aerosols are mostly carbonaceous compounds with a small fraction of inorganic compounds (Chen et al., 2017). Smoke aerosols form from the combustion of plants, forests, and other materials. As seen in Table 1.1, smoke aerosols are less than the others in the total aerosol load, but they can significantly affect living things and climate. Unlike other aerosols, BC and soot are the most well-known smoke aerosols causing the heating of the atmosphere.

Natural sources of aerosols are mineral dust, sea salt, soil debris, rock debris, forest fire, biogenic, volcanic eruptions, and vegetation gases (Rap et al., 2013). Sea salt and dust are the most abundant natural aerosols (Andrews, 2010). Dust particles are primarily insoluble solid particles driven by wind in areas without vegetation, desert areas, and soil

surfaces. Soil moisture, precipitation, and humidity affect dust mixing in the atmosphere. The wind produces sea salt aerosols on the ocean's surface (Calvo et al., 2013). Relatively larger particles settle back to the ocean surface, and other smaller particles (0.1 to 1 μm) mix with the atmosphere and stay in the atmosphere for a long time. Additionally, some organic compound microorganisms, the precursor sources of sulfate aerosols, can be found on the ocean's surface and released into the atmosphere by the wind on the ocean's surface (Kommalapati & Valsaraj, 2009).

Viruses, pollens, bacteria, and spores can be listed as biological aerosols (Rap et al., 2013). The distribution of them may vary according to the season and region. They can travel long distances by the driving force of the wind. They can be seen in many different sizes; for example, viruses have 0.05–0.15 μm sizes, and pollen can reach 30 μm (Andrews, 2010).

During volcanic eruptions, particles such as dust, ash, metal oxides, and sulfurs are emitted into the atmosphere. Volcanoes, the most crucial mechanism in forming sulfur aerosols, can create a cooling effect due to the sulfur they emit into the atmosphere (Andrews, 2010).

Particles enter the atmosphere from the surfaces, clouds, or space (cosmic aerosol). In addition, gas-to-particle reactions can generate particles. The formation of aerosols relies on atmospheric and physical-chemical processes. In general, the formation mechanism and processes of aerosols can be seen in Figure 2.1. Aerosols have two formation mechanisms; they are either directly emitted into the atmosphere or formed from precursor gases. Directly emitted aerosols are called primary. Origin from precursor gasses is called secondary aerosols. As seen in Figure 2.1, physical (coagulation, condensation, sedimentation) and chemical (such as oxidation and hydrolysis) processes can change the size and chemical composition of the aerosols with time (Morawska, 2003). Anthropogenic activities and natural processes emit gases and particles into the atmosphere. Particle-based aerosols, described as primary, disperse the atmosphere with vertical mixing and wind. In contrast, gas-based secondary-type aerosols are formed due to chemical reactions. Secondary aerosol particles are also produced by physical processes such as condensing vapors of precursor gases and nucleation, which is the condensation process of a particle under supersaturated conditions. The precursor gases are generated mainly through anthropogenic sources like combustion processes and

traffic emissions; however, natural-based precursor gases are released by natural fires, volcanic eruptions, and ocean surface (Myhre et al., 2013).

Oxidation and hydration processes are important chemical mechanisms effective in the growth of aerosol sizes. Oxidation is one of the chemical mechanisms causing the aging of aerosols. Aerosols can also grow with water vapor related to relative humidity, which refers to the hydration of aerosols. Hydration of aerosols is vital in Cloud Condensation Nuclei (CNN) amounts, thus indirectly affecting the global climate (Vu et al., 2015). While hydration is particularly effective in the growth of sea salt aerosols, dust aerosols are not affected as most are composed of insoluble solid particles (Andrews, 2010).

Primary aerosols are divided into inorganic and organic based. Inorganics are comparatively large and have short atmospheric continuances, generally only many days. Ocean spray and dust are examples of this group. Organic primary aerosols are created from the combustion of fossil energies, wood and biomass burning, other anthropogenic sources, and soil. Secondary aerosols are smaller and have larger atmospheric continuances than primary aerosols, generally days to weeks.

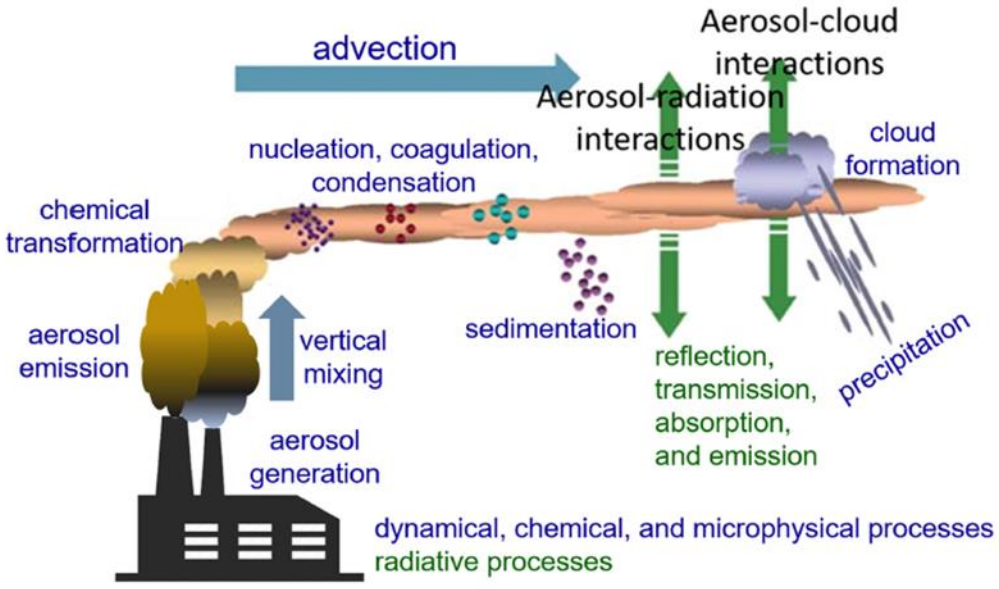

Figure 2.1. Formation processes and mechanisms of aerosol (Kuniyal & Guleria, 2019).

Physical properties of aerosols can be listed as number, shape, and size based on diameter, surface area, mass, size, and electrical charge distribution. Aerosols can have various

sizes ranging from 0.001 to 100µm. Fog and mist have a length of 10 µm – 100 µm, dust particle size of around 0.5 µm, and fume usually <0.05mm (Morawska, 2003).

Atmospheric aerosol distributions are characterized according to size as nuclei or fine mode, accumulation mode, and coarse mode. Nuclei mode with a diameter ranging from 0.005 to 0.05 µm and a volumetric geometric mean size from 0.015 to 0.04 µm. Accumulation mode with a diameter ranging from about 0.05 µm to 2 µm and having a volumetric geometric mean size from 0.15 to 0.5 µm. Coarse mode with a diameter ranging from about 2 µm to 100 µm diameter and a volumetric geometric mean size from 5 to 30 µm (Whitby, 1978). The fine, accumulation, and coarse mode aerosols originate, transfer, and are removed with different mechanisms and have different optical properties, detection methods, and control techniques (Myhre et al., 2013).

The fine mode aerosols are emitted to the atmosphere through combustion processes, condensation, and nucleation of new particles. This mode consists of most atmospheric particles as numbers but has a small mass fraction and includes trace elements and toxic materials. The fine-mode particles can coagulate and become an accumulation mode. The accumulation mode aerosols are generated from the coagulation of fine mode aerosols, chemical reactions, and gas-to-particle conversion. In coarse mode, particles are generated mainly through mechanical processes and can sediment and wash out. Accumulation mode aerosols can remain in the atmosphere for long periods, and their removal efficiency is the least than coarse mode. In addition, the accumulation mode of aerosols is the major part of adverse health effects (Morawska, 2003). The differences in the origin and size of the modes have information on the type and impact of aerosols.

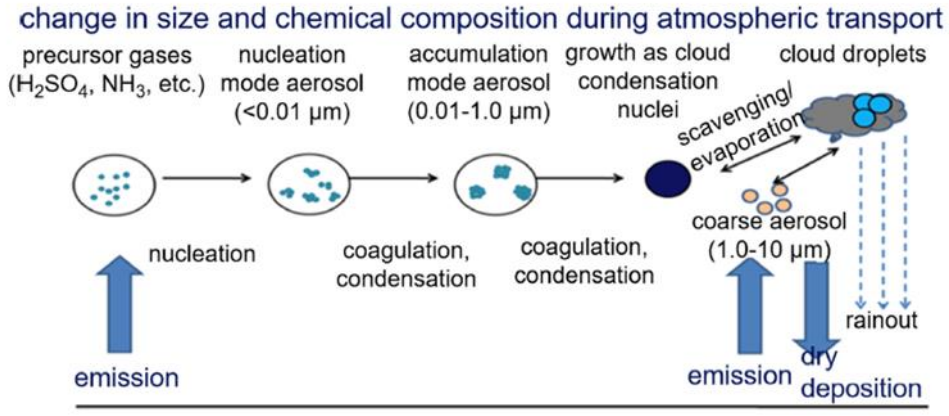

Figure 2.2. Change in size and chemical composition during atmospheric transport (Kuniyal & Guleria, 2019).

Aerosols' size and distribution change with formation and sink processes during transport, as seen in Figure 2.2. Aerosols can be removed by dry and wet deposition. Dry deposition results from gravity forces, collision, or diffusion, and heavier or bigger particles are deposited more quickly than others. Wet deposition is precipitation's removal of particles with water droplets (Cox, 2005). Fog and clouds can be another removal mechanism; particles are deposited in that system by dissolving them (Slanina, 2004). Those removal mechanisms cause a lifetime of aerosol to a week approximately (Cox, 2005). Wet deposition is the major part of aerosol removal in the atmosphere, whereas dry deposition plays a less critical role (Pöschl, 2005).

2.2. Optical Properties and Effects of Aerosols

The optical properties of atmospheric aerosols differ due to composition, shape, size, and concentration. Aerosols can absorb and scatter incoming solar radiation. The extinction is the sum of light absorption and scattering of incoming radiation. In the visible range of the light spectrum, scattering is the most noticeable in the extinction of incoming solar radiation (Kokhanovsky, 2008). Aerosols affect radiative balance directly with the extinction of incoming radiation and indirectly with their role in cloud formation and biogeochemical cycles like water, carbon, and sulfur (Pöschl, 2005; Rap et al., 2013).

While all aerosols scatter light, only some can absorb light. Many aerosols can absorb solar radiation; however, all atmospheric aerosols scatter solar radiation. Scattering aerosols have a cooling effect on the atmosphere because they increase the return of incoming light while absorbing aerosols have a warming effect because they increase the amount of energy remaining in the atmosphere (Myhre et al., 2013). Due to the scattering effect, aerosols negatively affect the earth’s radiative balance. Despite the net cooling effects, there are absorbing aerosols such as soot and BC cause heating in the atmospheric layer. Overall, aerosol pollution’s impact on climate will counter atmospheric greenhouse gases. Although greenhouse gases are expected to affect wildly everywhere, the effect of aerosol pollution is expected in regional terms regional term (Kommalapati & Valsaraj, 2009). Controversy continues as what the overall effect of aerosols.

The light scattering effects of aerosols vary depending on their size, wavelength, and scattering index. The most important optical properties are AE, scattering and absorption coefficients, and AOT. AOT refers to the aerosol load along a column, which is an excellent indicator for defining aerosol load in a region. AE is a parameter that shows the

change in the AOT value depending on the wavelength. The scattering index of aerosol varies with its chemical composition and wavelength. It is defined as m=n-ik, where n is the real index, k is the imaginary index, i is the number of components, and m is the refractive index. The optical depth of the aerosol is calculated using Equation (1):

$$\lambda = \varepsilon_{\text{ext}} {}^{*}\text{z} \tag{1}$$

Where ε_{ext} is the extinction coefficient, the sum of absorption and scattering coefficients as seen in Equation

(2), and z is the distance from the measurement point to the top of the atmosphere.

$$\varepsilon_{ext} = \varepsilon_{abs} + \varepsilon_{sct} \tag{2}$$

Scattering coefficients are calculated in two ways: Rayleigh and Mie theories. Rayleigh's theory is applied to small and non-absorbing particles, whereas Mie's theory applies to all sizes and both for absorbing and non-absorbing coefficients. Using Mie's theory, absorption coefficients can be calculated (Kokhanovsky, 2008). Rayleigh's theory defines molecular scattering, whose size is much less than the wavelength, and Mie's theory explains particle scattering (Andrews, 2010).

Aerosols act as CNN and change cloud properties and lifetime. In the earth's radiative balance, clouds also play a role in the albedo effect. Clouds scatter solar radiation; therefore, expansion or pollution due to aerosols causes more scattering of solar radiation or more albedo effect. On the other hand, smaller cloud droplets cause a more extended cloud lifetime and increase the amount of scattered radiation (Lohmann, 2007). In addition, clouds play a role in the hydrological cycle and thus can affect deposition properties.

Aerosols are also considered atmospheric pollution. Therefore, they affect human health and visibility. Scattering aerosol can affect visibility by reducing the lower troposphere's incoming solar radiation and temperature (Kommalapati & Valsaraj, 2009). Aerosols can affect human health in various paths based on their composition and size distribution.

Inhalation of aerosols causes respiratory problems and may exacerbate the condition in people with heart disease, especially aerosols like PM_{10}, generated from combustion and industrial process traffic originated. Smaller fine particles can penetrate the lungs and be found in other organs; ultrafine particles can be found in blood circulation and the brain's nerves (Pöschl, 2005; Kennedy, 2007). In a study in London (Atkinson et al., 1999), aerosols like PM_{10}, CO, and BS significantly contribute to cardiovascular diseases, and PM_{10} and SO_2 concentration increases respiratory infections in children. Biogenic aerosols such as viruses, pollens, spores, and bacteria can affect human health. We see one of the most apparent health effects of aerosols as allergic diseases such as pollen allergy (Mauderly & Chow, 2008). They also adversely affect the immune and defense systems (Pöschl, 2005). In conclusion, aerosols significantly adversely affect human health and global climate due to their optical properties.

2.3. Monitoring of Atmospheric Aerosols

Aerosol composition and size vary due to their sources and formation mechanisms. Therefore, there are many methods or instruments for the classification of aerosols. Aerosols are detected by on-site (real-time) measurements, active or passive sampling, continuous measurements, or sampling from flow measurements. Several methods generally measure aerosols' physical properties and chemical and biological composition.

Measured physical properties are listed as number concentration, particle mass concentration, the diffusion-limited mass transfer rate of a gas to aerosol particles, and optical properties (McMurry, 2000). Aerosols' physical measurement techniques can be grouped as mass measurement, number concentration measurement, and size distribution measurement. Mass measurements are done in static (the sample collection) or dynamic methods. Aerosols can be collected by filter, gravitational, diffusional, and electrostatic deposition in static mass measurement techniques. The dynamic mass measurement techniques include the piezoelectric mass monitor, tapered-Element Oscillating, microbalance method, optical techniques, and aerosol photon nephelometer. Number concentration measurement techniques are condensation nucleus counters and aerosol electrometers. Optical particle counters, electrostatic classifiers, and diffusion batteries are size distribution measurement techniques. Particle size distribution measurement, generally made by distribution, is usually obtained by dynamic aerosol detection technique with a size classification technique (Morawska, 2003).

Although the size of the same particle is expected to measure the same value, different measurement techniques can result in different sizes for the same particle. In some particle shape, density, and size methods, such as devices like impactors and aerodynamic particle sizers, the measured value depends on the refractive index of particle, shape, and size in optical size measurement techniques (McMurry, 2000). The classification method missions can be chosen considering the application purpose and scientific concern.

Light extinction and AOT are the measured optical properties in aerosol distribution monitoring. Light extinction and AOT are measured using passive or active devices. Sun photometers are passive devices, and active devices are laser photometers or LIDAR (Laser Imaging Detection and Ranging). Besides, light extinction is measured separately as light scattering and absorption coefficients with nephelometers or photometers (Hidy, 2019).

Satellite remote sensing and ground-based observations have recently become widespread to monitor aerosol distribution. Remote sensing is the measurement by a recording device that is not in physical or close contact with the object under investigation. In satellite remote sensing, electromagnetic radiation is detected after interaction with the atmospheric components (Payan et al., 2005). Spectroradiometers, multichannel and broadband radiometers, sunphotometers, and spectrometers are ground-based instruments for monitoring aerosols. Aerosol spectrometers take air with particles to calculate the number and volume concentration from light scattering (Verma et al., 2019). A radiometer measures solar radiation directly from the entire sky; a sun photometer measures solar radiation directly from the sun. Direct sunlight measurements are made by two kinds of detectors: broadband detectors which measure total sunlight, and selective multichannel sensors, which measure a particular range of wavelengths (Brooks, 2008). Sunlight measurements based on the well-known Beer's law:

$$I_\lambda = I_{0\lambda}\exp(\tau_\lambda m_{air}) \quad (3)$$

Where: I is the measured intensity, I_0 is the intensity at λ, and m_{air} is the relative air mass.

Historically, handheld sun photometer developments started with Volz's (1959) studies. In this work, Volz proposed a photometer with a 500 nm filter and selenium detector that measures AOT at 440, 500, and 640 nm. After this, he added a 940 nm filter to his device to measure water vapor absorption. Then he developed his photometer (F. E. Volz, 1974) by adding new filter channels and silicon photodiode detectors inside selenium. These studies were followed by solar photometers with led filters developed by Mims (1992). then the most widely used MICROTOP II by Mims and his colleagues (Morys et al., 2001) and CIMEL by Cimel Electronique (*CE318-T - Sun Sky Lunar Multispectral Photometer | Cimel Electronique*, n.d.) ground-based sun photometers were developed. MICROTOP II sunphotometer is a five-channel (440, 500, 675, 870, and 936 nm) handheld device measuring the total column and giving ozone content, AOT, and water vapor (Verma et al., 2019). The CIMEL 318A is a multiwavelength radiometer with two detectors, as seen in Figure 2.3. One detector measures the sun's irradiation, and the other the sky's radiation. Measurements are carried out for direct sunlight in 8 different wavelength ranges between 340 nm to 1020 nm every 15 minutes and for sky radiation at 440-670-870-1020 nm wavelengths in the daytime. With CIMEL sun photometers and the AOT values, the microphysical properties of the aerosols, such as the size distribution, began to be measured (Holben et al., 1998). NASA founded the AERONET (AErosol RObotic NETwork) project. This network provides optical properties such as AOT and AE detected by CIMEL sunphotometers globally.

Since F.E Volz (1959), the method used has not changed; the extinction light detected according to a combination of Beer-Lambert and Bouguer Laws:

$$V_\lambda = V_{0\lambda} \mathrm{d}^2 \exp(\tau_\lambda m) * t \qquad (4)$$

Where: V is the digital voltage at λ , V_0 is the extraterrestrial voltage at λ, m is the optical air mass, d is the proportion of average Earth-Sun distance, τ_λ is the total columnar AOT. All developed devices measure the total AOT using this formula.

Figure 2.3. CE318 photometers(*CE318-T - Sun Sky Lunar Multispectral Photometer | Cimel Electronique*, n.d.)

3. METHOD

All the measurements reported as the scope of this thesis were made with Sun-sky radiometers.

3.1. Study site and measurements

The AOT and AE values used in this study are taken from the AERONET for Erdemli station.

3.1.1. Erdemli Station Data

Erdemli station is located at 36.57°N and 34.26°E coordinates in the south of Turkey on Eastern Mediterranean, as seen in Figure 3.1. Different aerosols influence this station due to its location. It is thought that different kinds of aerosols, such as sea salt aerosols due to its proximity to the sea, urban aerosols due to population density and being an industrial area, and dust aerosols due to dust transport, are effective in the region.

Figure 3.1. Erdemli station location on Google Earth (36.57°N and 34.26°E)

In Turkey, there are three AERONET stations; TUBITAK_UZAY_Ankara, and IMS-METU-ERDEMLI. There are only 15 days in the Tuz_Golu station, approximately one year of measurement results in TUBITAK_UZAY_Ankara, and 14 years of data in the Erdemli station. Aerosol classification was carried out for the Erdemli station, which represents the region that is the subject of the thesis and has high data availability

.

AERONET relies measurements at 8 different wavelengths (340, 380, 440, 500, 675,870, 1020, and 1640 nm) each lasting one-second direct sunlight measurements. Direct sunlight measurements last 10 seconds and are repeated thrice at 30-second intervals every 15 minutes (Holben et al., 1998). In addition to those 8 wavelengths, measurement is conducted at 935 nm to calculate the optical depth of the water vapor. From Equation (4), the total columnar optical depth for each wavelength is detected. Then, the total optical thickness values are used to calculate AOT values in given wavelengths by the following equation:

$$AOT(\lambda) = \tau_\lambda(total) - \tau_\lambda(Rayleigh) - \tau_\lambda(H_2O) - \tau_\lambda(O_3) - \tau_\lambda(NO_2) - \tau_\lambda(CO_2) - \tau_\lambda(CH_4) \quad (5)$$

$\tau_\lambda(O_3)$ is calculated by absorption coefficient concentration derived from Total Ozone Mapping Spectrometer and ozone air mass. $\tau_\lambda(H_2O)$ derived from measurement at 935 nm, $\tau_\lambda(NO_2)$ is derived by absorption coefficient, concentration derived from Ozone Monitoring Instrument. $\tau_\lambda(CO_2)\ and\ \tau_\lambda(CH_4)$ are calculated by assuming constant absorption coefficient and concentration based on the HITRAN (Giles et al., 2019). $\tau_\lambda(Rayleigh)$ derived from pressure of measurement site and optical air mass (Holben et al., 1998).

AERONET releases three levels of data: Level 1.0, Level 1.5, and Level 2.0. In the present version (version 3), Level 1.0 contains prescreened data, Level 1.5 contains cloud-screened data with anomaly checks provided on the instrument, and Level 2.0 contains cloud-screened and automatic data quality-controlled data. With the development of version 3, there is no need for data quality to be checked by the researchers (Giles et al., 2019). In this study, version 3 level 2.0 data has been used for chosen station. In level 2.0 cloud screened, quality-checked AOT values were extracted and used at 440,675, 870 nm and α(440-870), and α(440-675) values. α(675-870) is calculated from AOT values at 675 and 870 nm using Equation (11). The difference of Angstrom Exponent (Ǽ) is calculated as the difference between α(440-870) and α(675-870). AOT at 675 nm values class is classified by grouping them according to their number.

3.2. Aerosol classification algorithm

An empirical formula was proposed by Angstrom (1929) to estimate the spectral dependence of atmospheric extinction caused by aerosols.

$$\frac{\beta}{{\lambda_1}^{\alpha}}\ loge = log\frac{T_1}{U_1} \tag{6}$$

$$\frac{\beta}{{\lambda_2}^{\alpha}}\ loge = log\frac{T_2}{U_2} \tag{7}$$

$$\alpha = -\frac{log\dfrac{logT_1 - logU_1}{logT_2 - logU_2}}{log\lambda_2 - log\lambda_1} \tag{8}$$

Where β is the absorption coefficient at wavelength 1 μm, T_1 and T_2 are the vertical transmissions calculated from molecular scattering at λ_1 and λ_2 . U_1 and U_2 are the observed transmissions λ_1 and λ_2. Shifrin (1995) gave a general definition of AE, as seen in Equation (9).

$$AOT_\lambda = \beta\lambda^{-\alpha} \tag{9}$$

Where β is the AOT at wavelength 1 μm which is known as Angstrom's turbidity coefficient. Equation (9) can be rewritten in logarithmic form as:

$$InAOD_\lambda = -\alpha In\lambda + In\beta \tag{10}$$

By rationing Equation (10) at two different wavelengths and taking the logarithm, AE can be expressed from spectral values of AOT or the negative slope of AOT_λ and wavelength graph in logarithmic scale:

$$\alpha = -\frac{dInAOD_\lambda}{dIn\lambda} = -\frac{In(\frac{AOD_{\lambda_2}}{AOD_{\lambda_1}})}{In(\frac{\lambda_2}{\lambda_1})} \quad (11)$$

AE has valuable information about the particle size distribution of aerosols. The relationship between AE and particle size distribution is explained by Junge (1955) with the help of the number density (N) of aerosols as a function of radius(r):

$$\frac{dN}{d(Inr)} = cr^{-\upsilon} \quad (12)$$

Where dN is the number concentration of aerosols with radii between r and dr and c, υ are fitting parameters. c is a constant relying on physical characteristics ,and the slope of the radius distribution curve determines υ. This classification is helpful for nonabsorbing aerosols however is not valid for absorbing aerosols or small values of AE. Numerous study has investigated that multimodal lognormal distribution is more related to aerosol size distribution (Davies, 1974; Whitby, 1978):

$$\frac{dV(r)}{dInr} = \sum_{i=1}^{n} \frac{C_i}{\sqrt{2\pi}\sigma_i}, \exp[\frac{-(Inr - InR_i)^2}{2\sigma_i}] \quad (13)$$

Where C_i is the particle volume concentration, σ_i is the variance of each mode, R_i is the geometric mean radius, and n is the number of aerosol modes.

The extinction of a polydisperse distribution of aerosols can be calculated by using Equation (13):

$$AOT_\lambda = \int \frac{3Q_{ext}(m, r, \lambda)}{4r} \frac{dV}{dInr} dInrdZ$$

(14)

Q_{ext} is the extinction coefficient calculated using Mie theory for spherical aerosols according to the radius, wavelength, and refractive index. Z is the atmospheric column height.

AE values between 0 and 1 indicate that the coarse mode is dominant, and values greater than two generally indicate the fine mode (Holben et al., 1998). Values near zero indicate desert sand, while values greater than two are associated with a new smoke particle with accumulation mode and urban aerosols (Kaufman, 1992)(Basart et al., 2009). Although AE has valuable particle size distribution information, combining coarse and smaller fine-mode particles can have the same AE value as a fine-mode particle. It isn't easy to interpret the size by looking only at AE, especially for intermediate values such as 1 to 2. In addition, the AE value alone does not give information about the fraction of the modes.

AE also depends on wavelength. A second-order polynomial fit of the AE can show a relationship between the extinction of light by aerosols with varying wavelengths. (Eck et al., 1999):

$$InAOT(\lambda_i) = a_0 + a_1 In\lambda_i + a_2 (In\lambda_i)^2 \quad (15)$$

The coefficient a_2 represents the curvature of the AE. The curvature represents the change rate of the slope of the Inλ to Inα graph. In other terms, the curvature can be calculated from the following equation (Kaskaoutis et al., 2007):

$$\alpha'(\lambda i) = \frac{d\alpha}{dIn\lambda} = \left[\frac{2}{\lambda(i+1) - \lambda(i-1)}\right]\left[\frac{In\tau(i+1) - In\tau(i)}{In\lambda(i+1) - In\lambda(i)} \frac{In\tau(i) - In\tau(i-1)}{In\lambda(i) - In\lambda(i-1)}\right] = -2\alpha_2 \quad (16)$$

Equation

(16) shows that calculating the slope change rate requires at least three different wavelengths and AOT values. In previous studies (Kaufman, 1993; Eck et al., 1999), it is found that negative curvature represents size distribution dominated by fine mode;

positive curvature represents size distribution with a remarkable, coarse mode fraction. Another study (Kaskaoutis et al., 2007) found that the curvature depends on the differences between AE values rather than the slope of the Inλ to InAE graph. Also, they observed that in negative curvature, the change rate of α is more remarkable at longer wavelengths; in positive curvature, the change rate of AE is more remarkable at shorter wavelengths.

The AE and the curvature of the AE have valuable information about size distribution and dominated mode of the distribution, but. However, for further information, not only the distribution's dominated mode but also the coarse and fine modes' weight fraction should be investigated. In a recent study, Schuster et al.(2006) investigated the connection between the contribution of fine mode to total aerosol volume and AE. In another study which is the main frame of this thesis, Gobbi et al. (2007) created a new graphical method, as shown in Figure 3.2, for the classification of aerosols based on their optical properties with the help of AE, the curvature of angstrom exponent(Á), and fixed fine contribution to the total aerosol volume. The visual concept in Figure 3.2 is calculated from theoretical values and used as a reference point to analyze the contribution of fine mode to total and aerosol size distribution.

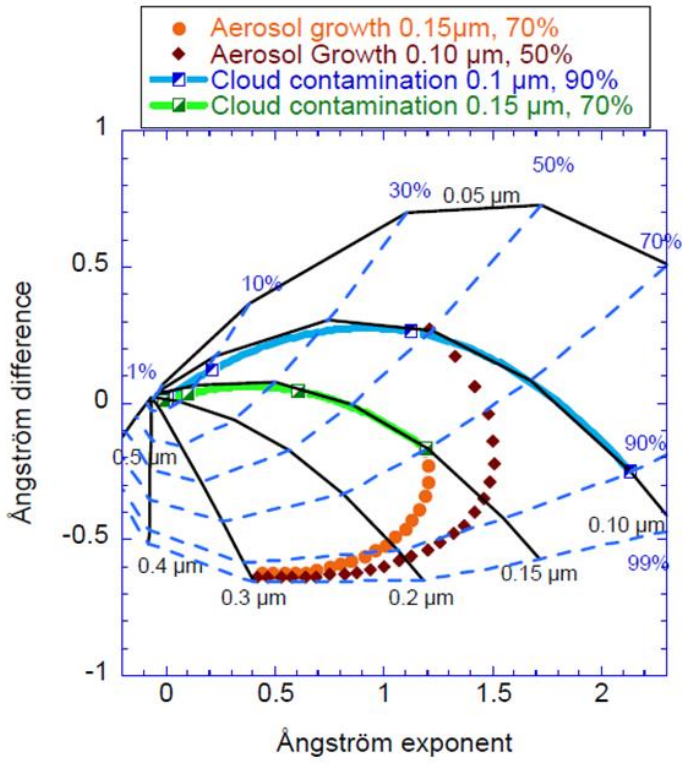

Figure 3.2. Graphical Framework-1 (Gobbi et al., 2007)

The fine mode radius ranges between 0.05 μm to 0.5 μm, as seen in Figure 3.2. The fractional contribution of fine mode is taken as 1,10,30,50,70,90,99 percent. The coarse mode radius is taken as 0.75 μm, 1 μm, 2 μm, and 4 μm. By combining these data, bimodal size distribution is calculated according to Equation (13) by switching dV(r) to $4/3\pi r^3 dN(r)$ to obtain number density. Since the change in coarse mode size does not affect the Á in the used wavelength range and to obtain a single fine mode number fraction and fine mode radii reference line, the average of the coarse mode is calculated according to 4 different radii and used as coarse mode. In bimodal size distribution, each mode width has held constant at 1.5 for fine mode and 1.8 for coarse mode for each radius. AOT values at 440,675,870 nm of each bimodal size distribution are calculated as in Equation (14). In extinction calculations, the refractive index is used as 1.4-0.001i to represent typical urban aerosol. Then AE values at 440-870, 440-675 and 675-870 nm of each bimodal size distribution are calculated using Equation (11). Á values are calculated as the difference of AE values at 440-675 and 675-870 nm.

The solid black lines are created for fixed fine mode radius from calculated AE values at 440-870 nm and Á values as the difference of AE values at 440-675 and 675-870 nm. Blue dashed lines are created values for different fixed mode contributions to total from calculated values of AE and Á. These wavelengths are chosen to avoid ozone scattering aerosols' effect, and the AERONET channel has more accuracy at that range.

The decrease in AE happens due to many reasons. AE may decrease with large particles, cloud contamination, aging of small particles, or growth with humidity. The difference between these mechanisms can be observed with the help of the graphic used. Cloud contamination data was created by adding a new mode to size distribution as 10 μm and 15 μm particles with %90 and %70 fractions, respectively. The refractive index in extinction calculations for cloud contamination is 1.33-0.000i representing the water droplets. The spots where the effects of cloud contamination are seen are marked with squares for the fine mode contribution of 0,50,90 and 99 percent. Aerosol aging is calculated by incrementing fine mode radii with constant intervals of 0.01 μm. The initial diameter is 0.1 μm, and the values calculated according to the %50 ratios are shown in brown. The initial diameter is 0.15 μm, and the values calculated according to the 70 percent ratio are shown in orange.

Aerosols scatter or absorb light in more direct relation to their volume than their number (Schuster et al., 2006). For this reason, it is essential to separate them not only according

to their numbers but also according to their volumes. With this in mind, in a study by Quirantes et al. (2019), the new graphical method was put forward by calculating the volume ratio of the fine mode to the total with the parameters used by Gobbi et al. (2007). The difference between the two graphs, the lognormal size distribution was made with volume calculations instead of number density. The graph used to classify according to volume is given in Figure 3.3.

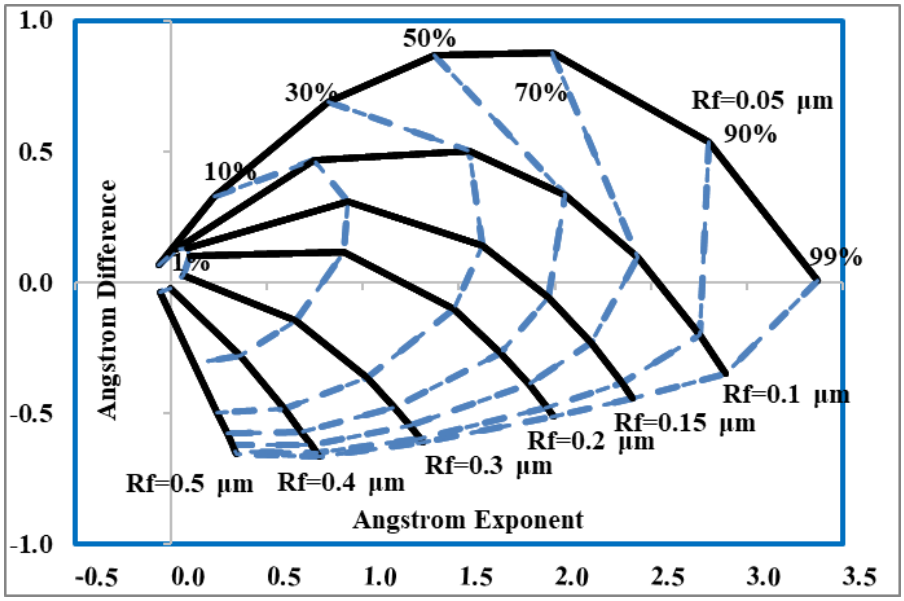

Figure 3.3 Graphical Framework-2 (Quirantes et al., 2019)

In the study by Quirantes et al. (2019), the effect of the shapes of the aerosols on the calculations of the extinction value was evaluated, and no significant difference was found between the non-spherical and spherical ones. Thus, it has been decided that using Mie calculations in extinction calculations is sufficient. In the same way, the refractive index, another variable that changes the optical properties, was examined. It was found that the changes in the refractive index in fine mode did not make a difference in total, but in the coarse mode, it caused a change in the graph. A new chart was created using the refractive index of the transported coarse mode dust, as seen in Figure 3.4.

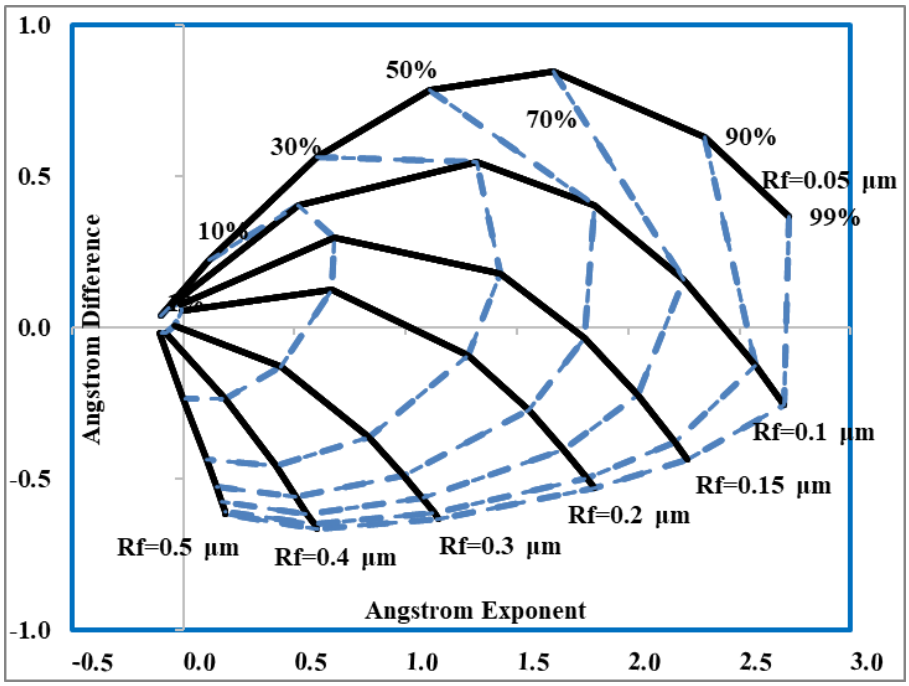

Figure 3.4. Graphical Framework-3 (Quirantes et al., 2019)

In this study, the measured data were placed in the graphs above, and analyzes were carried out. There are measurements of AE(440-870), AE(440-675), and AOT675 values for the Erdemli station. AE(675-870) data required to calculate the Á, AE values have been calculated from measured AOT values at 675 and 870 nm using Equation (11). Then AOT values at 675 nm were grouped in different ranges and placed on the graphs.

3.3. Cluster Analysis

To understand the contribution of transported aerosols to Erdemli's ambient air, trajectory analysis has been conducted for this study's annual and seasonal periods. 5-day back trajectories calculated with Hybrid Single-Particle Lagrangian Integrated Trajectory Version-4 (HYSPLIT_4) model described by Draxler & Hess (1998) for the selected time window of 11 years between 2010 and 2017 for 6-hour intervals and 1-hour retention time in each grid cell. Model run by Global Data Assimilation System (GDAS) 0.5º×0.5º gridded data obtained from US National Oceanic and Atmospheric Administration (NOAA), Air Sources Laboratory (ARL) READY meteorological data archive. 36.57°N and 34.26°E are the coordinates of Erdemli Station and were used as the starting point. 1500 m above mean sea level (AMSL) elevation was used to eliminate the impact of the Planetary Boundary Layer (PBL) seasonal changes above the land surface and to represent both PBL and lower Free Tropospheric air parcel transport. After completing each daily 0.5º×0.5º spatial and 1-hour temporal resolution trajectories, air parcels are

clustered according to their endpoint spatial variances to determine the main transport patterns that arrive at Erdemli. Plots are depicted as above-ground level (AGL) elevations with mean path percentages of each cluster in the annual and seasonal periods.

4. RESULTS AND DISCUSSION

The AOT measurements, which are at Level 2 for the Erdemli station in the AERONET data system, were published between 1999 and 2019. Unfortunately, the measurements between these years were not continuous; the months with the measurement numbers are shown in Table 4.1 according to the years. In some years, 12-month data is available; in others, this rate drops to 2 months. In analyses, years with data of 10 months or more were studied. The years selected by considering the data occupancy rates are 2000,2003,2004,2007,2008,2009,2010,2011,2013,2014,2016,2017. Since there were no AOT measurements at 870 wavelengths in the 2003 data, this year was not included in the study; the remaining 11 years were used.

Seasonal and monthly analyzes were carried out using the data from the selected 11 years. In previous studies in this region (Aslanoğlu et al., 2022), it was stated that dust transport to the area started in February, and the seasons were divided into four groups as follows: February-March-April as Spring, May-June-July as Summer, August-September-October as Autumn and November-December-January as winter. This study’s seasonal analyses were arranged according to this season's grouping.

Table 4.1. Data Availability by Month of Erdemli Station

Month/ Year	Jan	Feb	Mar	Apr	May	Jun	Jul	Aug	Sep	Oct	Nov	Dec
1999	0	0	0	0	0	0	0	0	0	0	305	642
2000	348	371	676	318	841	1169	1053	920	1091	802	890	627
2001	660	484	644	721	476	198	0	0	0	0	0	0
2003	61	262	630	420	500	0	61	68	42	0	0	0
2004	70	133	601	0	372	693	1271	1060	1063	1248	742	370
2005	0	0	0	800	899	1486	1206	1021	1133	1054	449	234
2006	342	196	20	199	21	0	0	0	0	0	0	605
2007	385	387	993	867	252	307	35	0	358	335	0	59
2008	554	887	785	774	1061	1632	1520	1213	972	654	434	339
2009	269	160	761	738	1307	1611	1461	1407	1057	1039	549	232
2010	138	277	555	398	253	207	1115	539	383	38	0	161
2011	359	202	237	0	0	885	1119	1282	1095	913	504	247
2012	66	0	9	0	105	134	0	0	0	0	196	303
2013	252	473	550	702	0	0	1095	1068	542	342	616	89
2014	88	792	59	0	53	1198	1217	1068	401	442	549	337
2015	0	0	115	606	425	161	162	0	0	0	512	622
2016	434	663	779	692	393	137	729	1371	1147	0	30	425
2017	118	392	673	745	823	869	866	1014	615	1151	560	503
2018	464	264	0	36	0	0	568	1300	1170	730	444	324
2019	301	582	679	170	299	0	0	0	0	0	0	0

4.1. Annual Analysis

Firstly, AOT and AE values of mentioned years have been examined. As seen in Figure 4.1, AOT_{675} values are mostly clustered between 0 and 0.5, at a maximum of 2.2 is observed. Values ranging from 0 to 2.2 show aerosol with different chemical properties and sizes throughout the year. It is seen that the AOT_{675} values started to increase after the 50th day of the year—this increase started in February and reached its maximum value between April and May. The lowest values were measured in January. It is thought that the sharp increase in AOT_{675} values between April and May indicates the change in aerosol type in the region. In Figure 4.2 AOT_{675} values are visualized as monthly mean using daily averages. As seen in this figure, the lowest monthly average was observed in January and the highest in August and April. With the month of February, an average value that is 2 times the previous month was observed. Thus, the opinion that dust transport to the region started with February was supported.

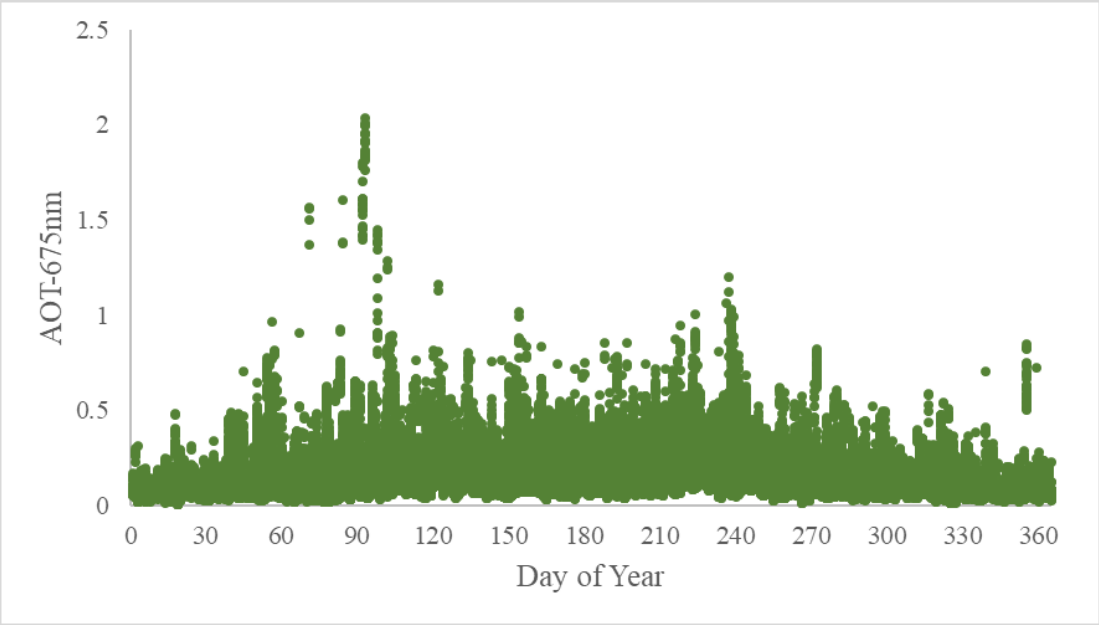

Figure 4.1. The daily variation of AOT_{675}

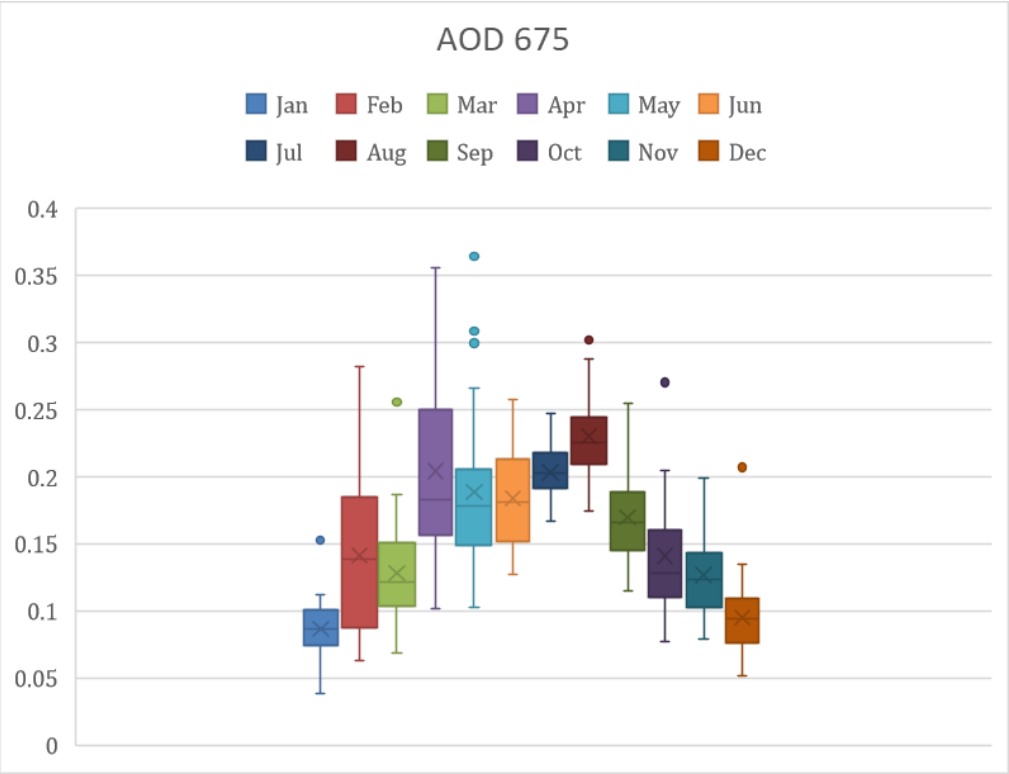

Figure 4.2. Monthly mean AOT_{675}

AOTs used in the study are visualized in Figure 4.3 and Figure 4.4 as monthly mean using daily averages. As in AOT 675, the lowest month in Figure 4.4 was January, while the highest was April and August. In the same way, the February value doubles the

January value, indicating the beginning of dust transport. On the contrary, a different distribution is observed in the AOT 440 graph, as seen in Figure 4.3. In previous studies (Schuster et al., 2006), they found that the fine mode scattering effect at small wavelengths, while the coarse mode scattering effect increases at high wavelengths. As expected, AOT_{440} measurements clustered between 0.8 and 1.4 due to fine mode contribution, while AOT_{870} measurements at higher wavelength clustered between 0.05 and 0.2. Since the effect of the fine mode is observed at small wavelengths, a distribution opposite to the other two wavelengths is observed.

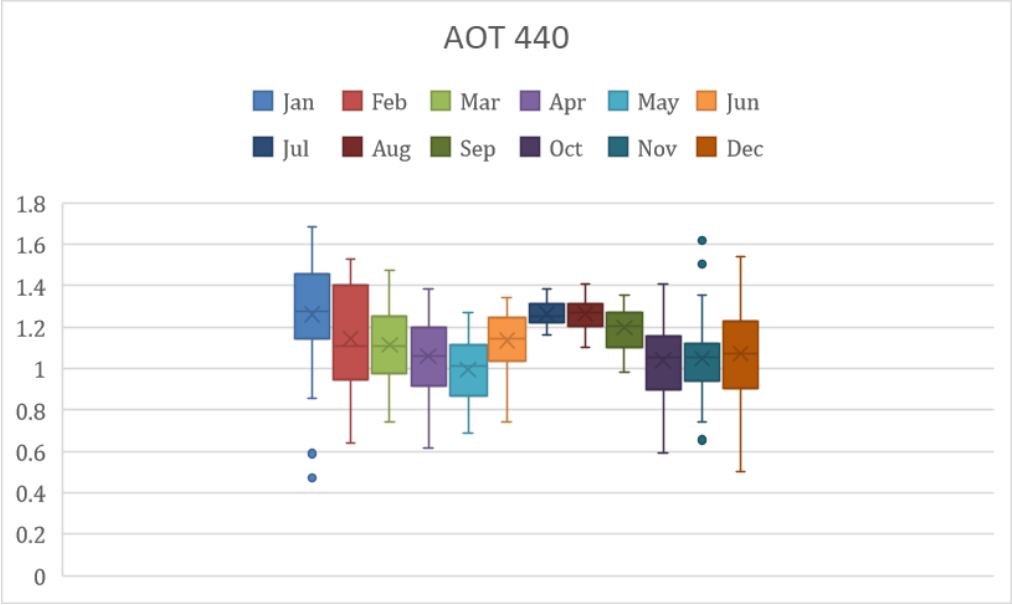

Figure 4.3. Monthly mean AOT_{440}

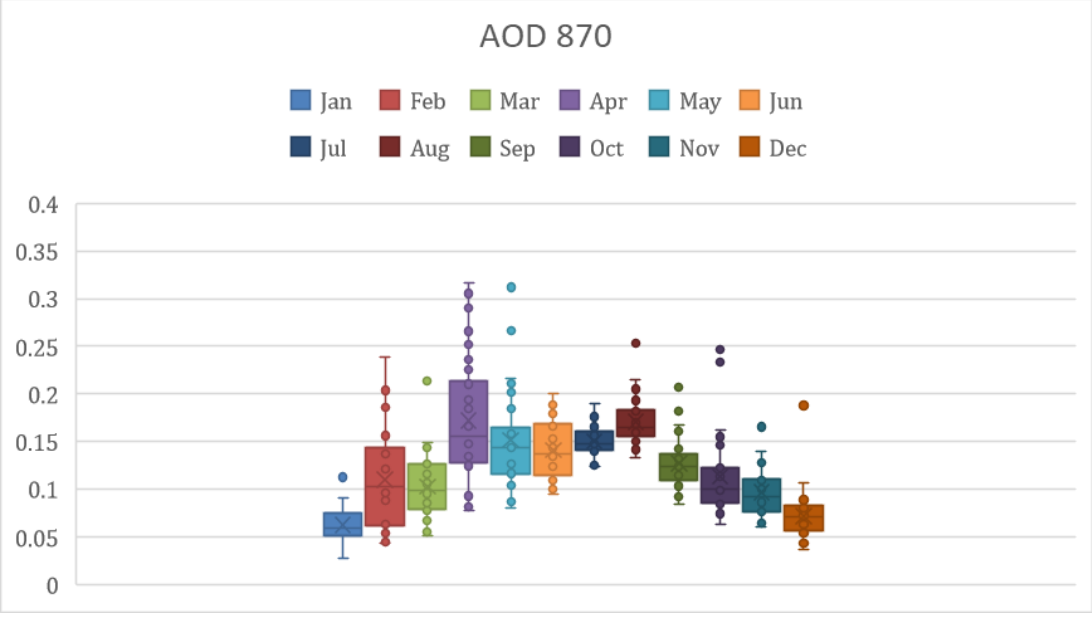

Figure 4.4. Monthly mean AOT_{870}

Daily variation of AE values can be seen in Figure 4.5. It is observed that measurements clustered in values greater than one, but values less than one are also observed throughout the year. Differences in a day between 0 and 2 indicate that aerosols of different sizes and characteristics influence the region. Points where AE values exceed 2 throughout the year, are clustered in the first four months and the last four months. Aerosols with an AE value greater than 2 are expected to be freshly formed smoke particles. According to this table, while freshly formed smoke particles are seen in the region throughout the year, the formation of these particles is significantly less in May, June, July, and August compared to other months.

Throughout the year, AE values between 0 and 1 indicates coarse-mode aerosols in the region. Considering the values associated with the presence of dust, which is close to 0, it is seen that dust is effective throughout the year and heavy dust transport started in February. The lowest values are seen in February, March, April, and May, and it is thought that dust transport to the region is high in these months. Although AOT values were as high as in spring, the decrease in AE values was relatively smaller in summer. This difference can be explained by the increase in the fine mode, as the region is affected by forest fires with the increase in temperature and dust transport in the summer months. Values between 1 and 2 throughout the year constitute the weighted part of the measurements and indicate that the accumulation mode is also effective in the region.

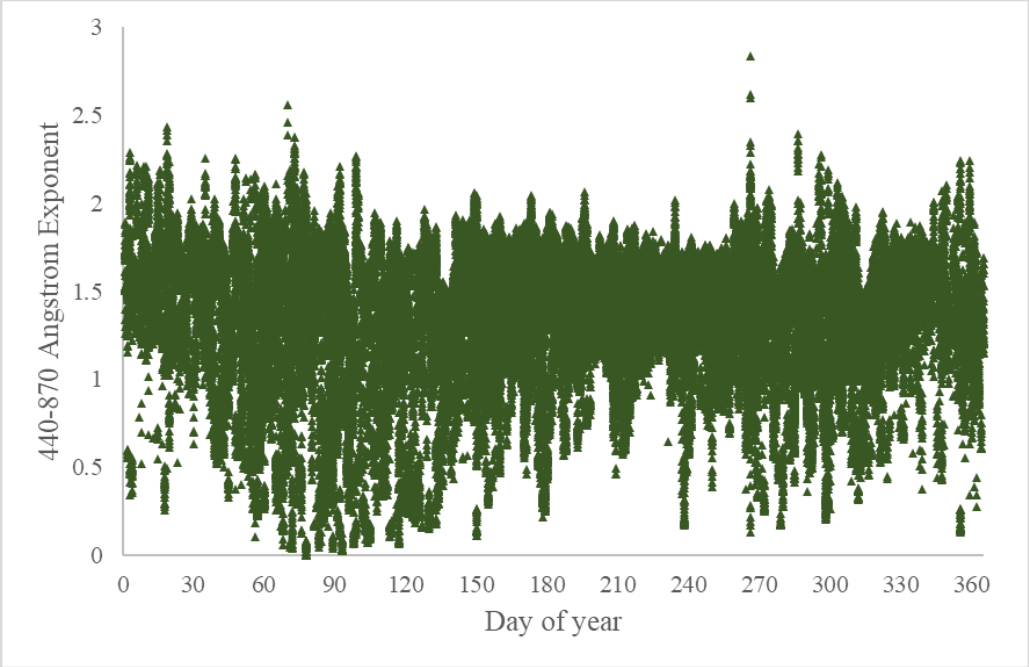

Figure 4.5. The daily variation of Angstrom exponent $\alpha(440,870)$

The graph created using 11 years is based on graphical frameworks are shown in Figure 4.6, Figure 4.7, and Figure 4.8. based on number fraction as seen in Figure 4.6, in general terms, as the effect of coarse mode increases, the R_f value increases, and number density contribution of fine mode and AE values decreases with the increasing AOT. For smaller AOTs between 0.15 and 0.4, the number density contribution of the fine mode ranges from 10% to 90%. Fresh smoke aerosols are observed in this AOT range where AE is greater than 1.5, and the number density contribution of the fine mode is 80-90% with negative Á that indicates fine mode dominance. The area where AOT is less than 0.7 and the number density contribution of the fine mode is greater than 70%, and AE greater than 1.5 with a negative Á indicates the presence of urban aerosols.

Size distribution shifts from 0.05-0.1 μm to 0.12-0.17 μm with increasing AOT, and the size distribution generally clustered between 0.05 and 0.15 μm radii. The number density ratio of fine mode to total varies between 10% and 70% of the radius between 0.05 and 0.1 μm. Between 0.1m and 0.15 μm, fine mode contribution varies from 10% to 90%. Thus, the fine mode number density increases with increased AE. It has been determined that there are two modes in these areas where mostly positive Á values are calculated. It can be said that while the coarse mode is dominant in values where AE is between 0.3 and 1, the fine mode is dominant in places greater than 1.

AOTs between 0.4 to 0.7 fit the 0.15 μm radii line, and the ratio of fine number density to total is between 1% and 90%. The increase of the fine mode located on the 0.15 μm line with increasing AE indicates that the accumulation mode is activated due to biomass-burning aerosols in the region.

AOTs from 0.7 to 1.5 clustered between 0.15 and 0.2 μm. In this range, AE values between 1 and 1.5 indicate biomass burning, and urban aerosols with accumulation mode and values lower than 0.5 show desert dust presented. The region with larger AOTs (from 0.7 to 3) and AE values between 0 and 0.3 where Á negative to lightly positive with a contribution of fine mode number density's 1% to 10% indicates the presence of desert dust in the region. This range shows that the area is exposed to heavy dust transport throughout the year, and the change according to the seasons and months is examined in the following sections.

Aerosol aging is observed in the area where the AE is approximately 1 for AOT between 1-1.5, and the radius is between 0.15-0.2 μm, n is between 70-90%.

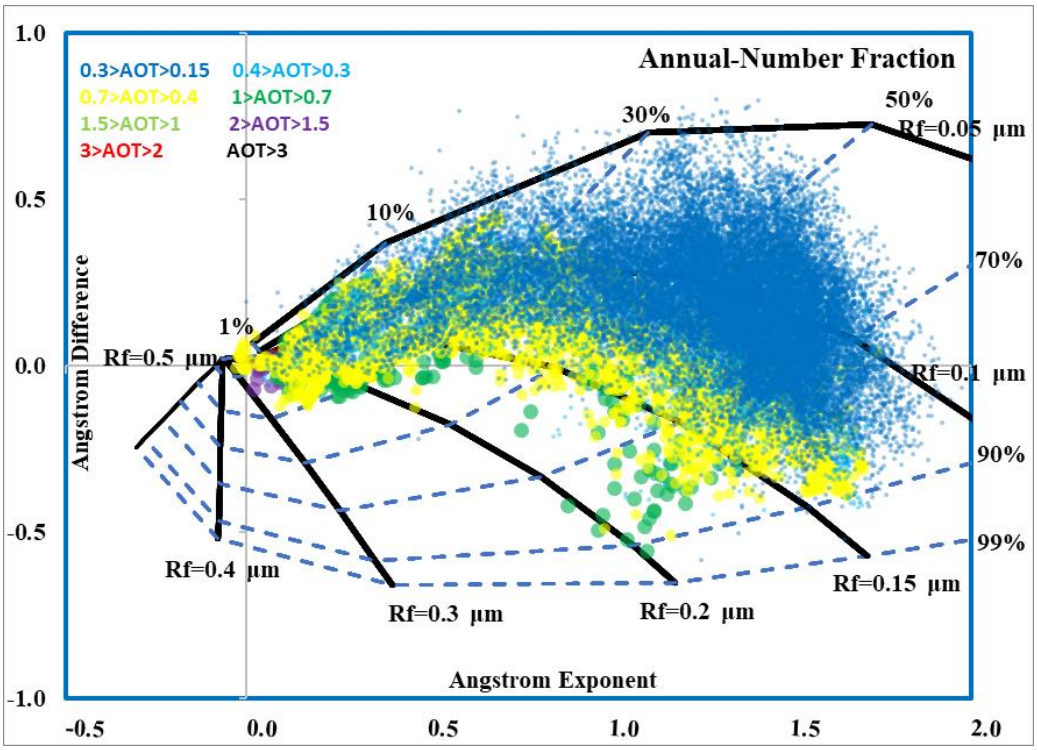

Figure 4.6. Annual aerosol classification by number fraction of fine mode

As seen in Figure 4.7, the fine mode volume contribution to the total does not exceed 50% throughout the year. Although the ratio of the fine mode to the total is significant in the number density analysis in Figure 4.6, this ratio shows a significant decrease when compared to the volume fraction. The presence of dust increases the volume effect of the coarse mode from 95% to 99%. In terms of volume, a large part of the aerosols of the region originates from the dust carried, and it constitutes the essential part of the aerosol load of the region. Even though the number density of the fine mode reaches 99%, the volume fractions get 50% at the most. Considering these data, the effect of the coarse mode can be seen easily in Figure 4.7.

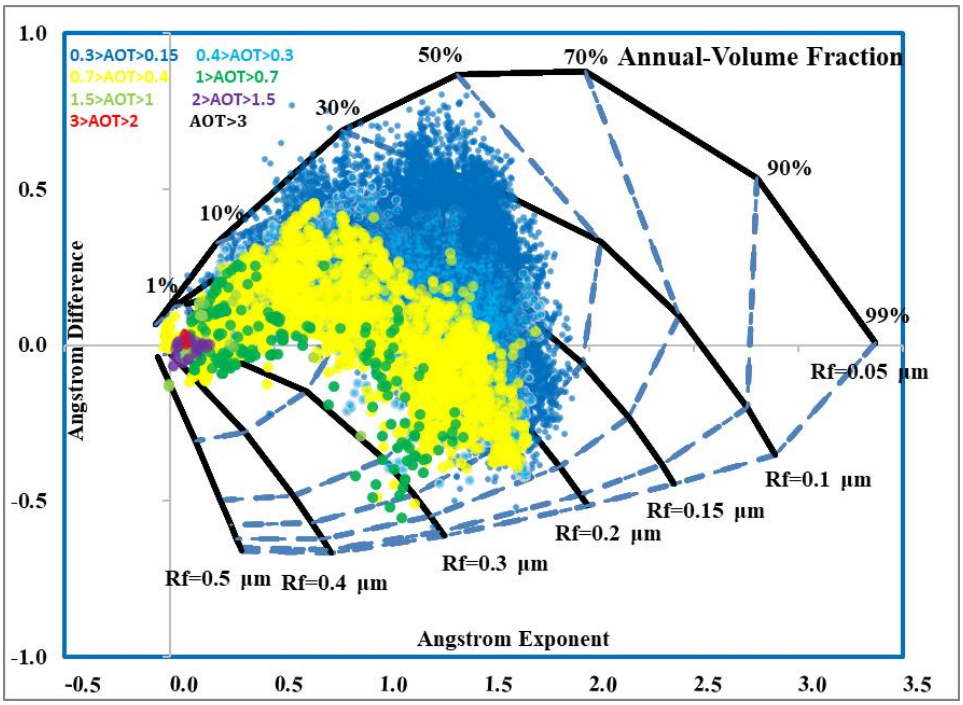

Figure 4.7. Annual aerosol classification by volume fraction of fine mode

According to Figure 4.8, where the effect of the dust is evaluated more accurately, there is a change in the volume fraction of the fine mode. The fine mode volume fraction increases slightly compared to the previous one, and the dust volume is between 90% and 99%. While dust volume in total varies between 95-100% in Figure 4.7, the volume fraction decreasing to 90% in Figure 4.8 shows that the refractive index of the coarse mode is effective. After the preliminary classification, it is seen that a unique graphic should be created for the species to be investigated to obtain precise results.

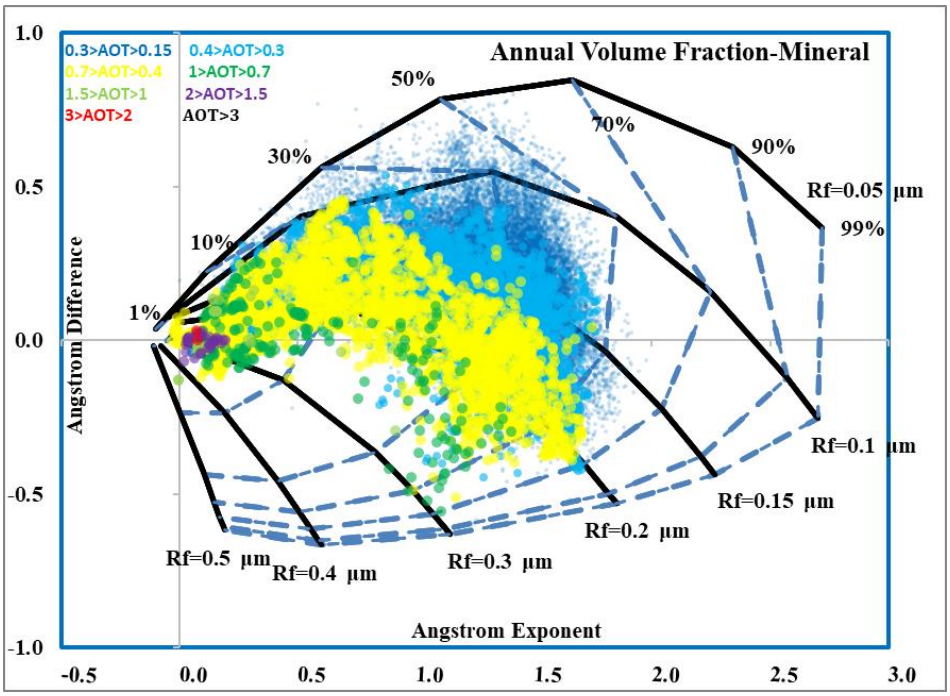

Figure 4.8. Annual aerosol classification by volume fraction of fine mode, mineral transported model

According to the classification, it is seen that there is dust transport to the region. In order to decide the transport routes, the wind profile of the region was determined. Considering that dust transport is effective up to a height of 1500 meters, the profiles were created considering this height. First, the general wind profiles for the region at 1500 m height were drawn, the required number of clusters was determined with the help of the graphic shown in Figure 4.9. In the profile to be created for the selected 11 years, since the change is significantly reduced after the 7, the number of clusters is determined as 7.

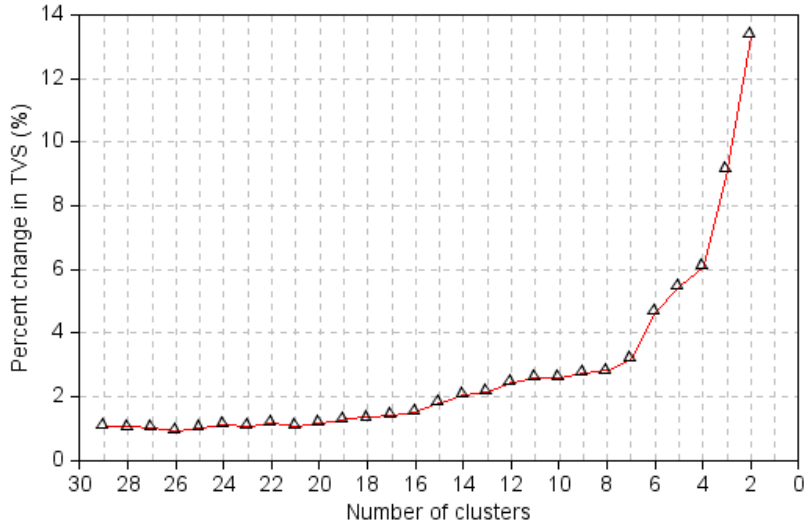

Figure 4.9. Number of Cluster graph in Erdemli in 1500 m height

The percentages of the wind for 7 clusters and the transportation routes to the station are shown in Figure 4.10. The profile with the highest percentage in the map is cluster 2, followed by cluster 5. The wind from the southwest (cluster 2) is considered the cause of dust transport to the region. As can be seen, some winds from the ocean cause sea salt aerosol load. There is urban aerosol transport along with the winds from Europe and northern countries to the region.

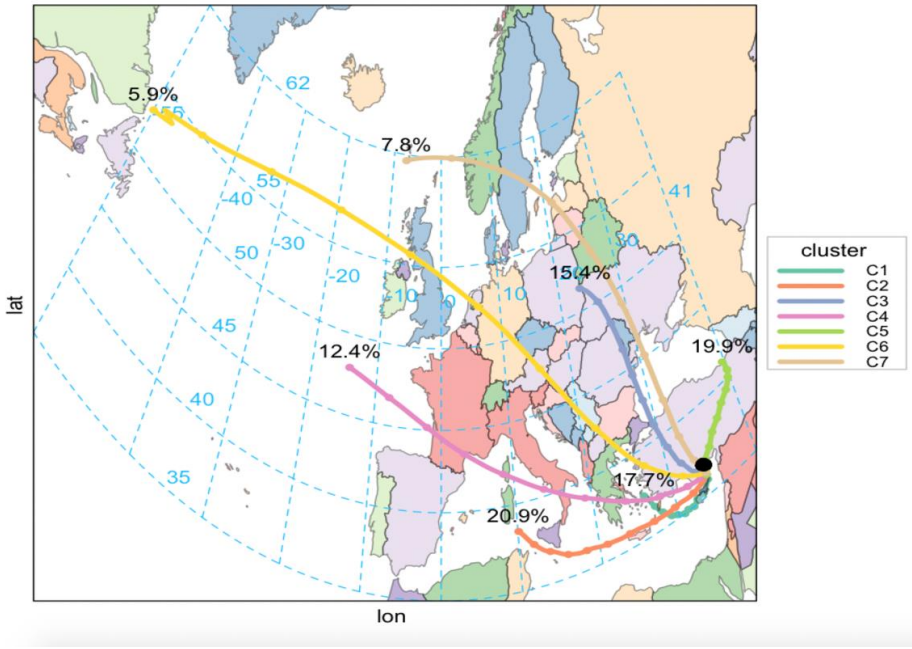

Figure 4.10. Cluster Analysis in Erdemli in 1500 m height

4.2. Seasonal Analysis

Aerosol types are classified according to the seasons in this section. Annual analyses show that the AOT reaches the highest values in the Spring, while the lowest ones are obtained in the Autumn. Significant increases in AOTs are observed, especially in the Spring and Summer. There is a significant decrease in values of AE even to 0 in the Spring, while considerable decreases are observed in the summer.

Figure 4.11, Figure 4.12, and Figure 4.13 include graphs of the Spring season. In Figure 4.11 number fraction of fine mode is seen. For smaller AOTs between 0.15 and 0.4, aerosol radii vary between 0.05 and 0.12 μm in areas where AE values are greater than 1, while the number density of the fine mode varies between 30% and 80 In these areas where Á is positive, two modes are considered active. It is seen that the fine mode is the dominant mode for AE greater than 1. Aerosol aging due to hydration is observed in the 0.12-0.15 μm radius range where Á is negative for this AOT range.

The greater AE and more extensive fine mode number fraction for the other relatively high AOTs between 0.4 and 0.7 indicate aerosols originating from biomass burning. Increasing AE with increased fine mode contribution indicates typical urban aerosols for this AOTs range. The number density of the fine mode varies between 30% and 80% at lower AOTs, while the number density of the coarse mode is 70% and 99% at higher AOTs. As in the annual evaluation, biomass and urban aerosol are also observed in the Spring.

The number density contribution of the coarse mode relies on between 90% and 99% for AOTs greater than 0.7. Higher AOTs with AE close to zero show the presence of dust. Since AOTs greater than 0.7 are clustered only in this region, dust transport is the reason for the AOTs to exceed 0.7.

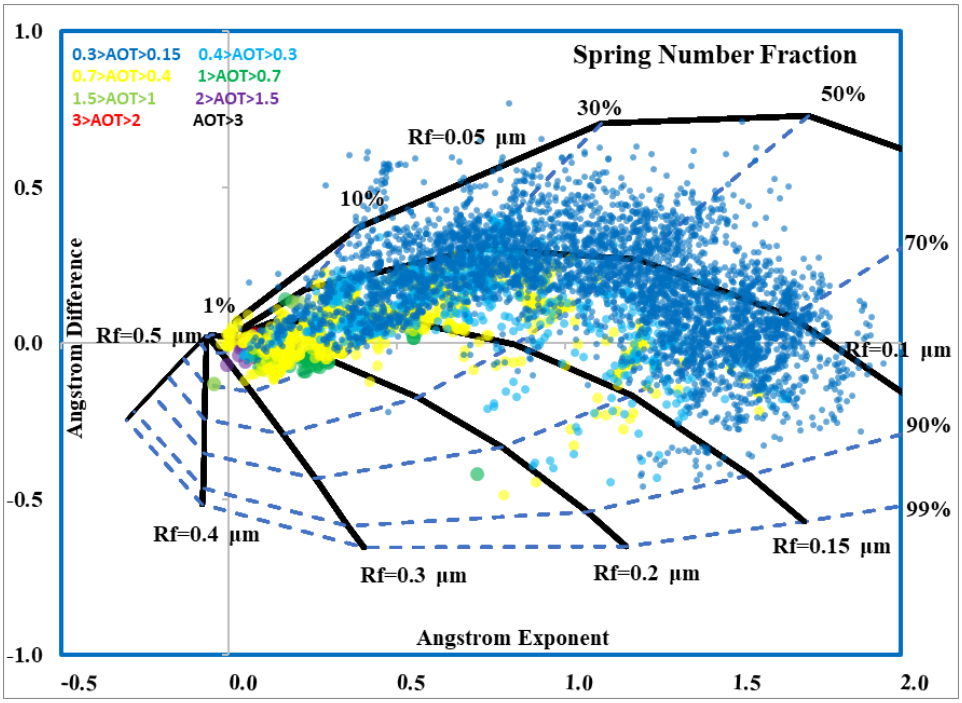

Figure 4.11. Seasonal aerosol classification by number fraction of fine mode-Spring

As seen in Figure 4.12, the volume fraction of the coarse mode in the area showing the presence of dust was seen in the range of approximately 97-99%. In this area, although the number density of the coarse mode is smaller than the volume fraction since the optical properties are more related to the volume, the most effective mode in Spring is the coarse mode, which is formed because of dust transport.

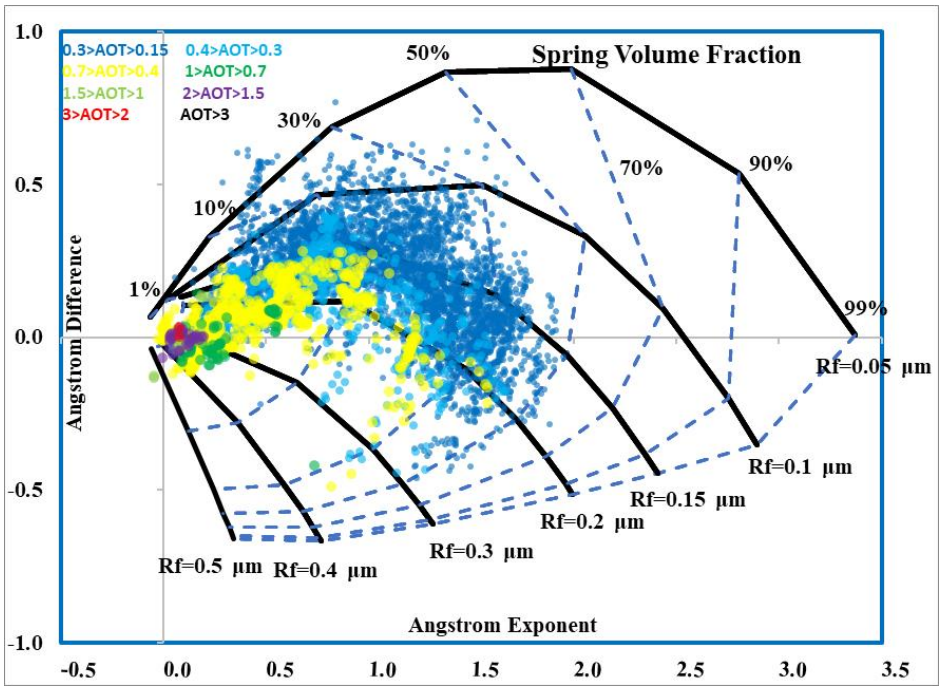

Figure 4.12. Seasonal aerosol classification by volume fraction of fine mode- Spring

In the analysis made according to the refractive index of the transported dust, as given in Figure 4.13, it was seen that some of the AOTs between 0.4 and 0.7 shifted to the dust transport area. From this point of view, it is thought that dust particles in the accumulation mode and the coarse mode are transported to the region in the spring.

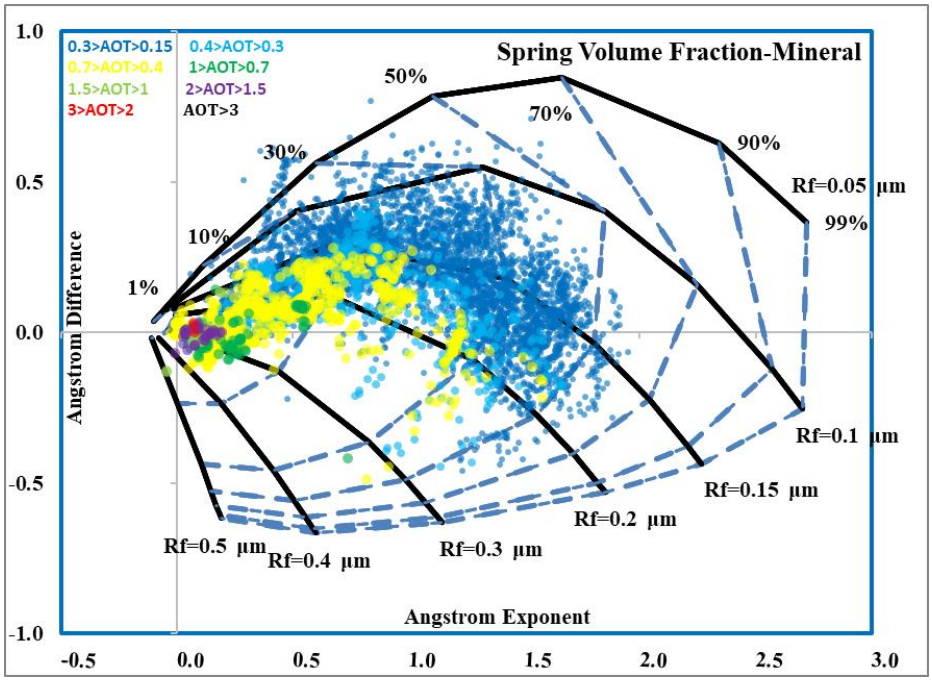

Figure 4.13. Seasonal aerosol classification by volume fraction of fine mode- Spring, mineral transported model

Before the general wind profiles for the region of Spring at 1500 m height were drawn, the required number of clusters was determined with the help of the graphic shown in Figure 4.14. In the profile to be created for the selected 11 years, the number of clusters is calculated as 9.

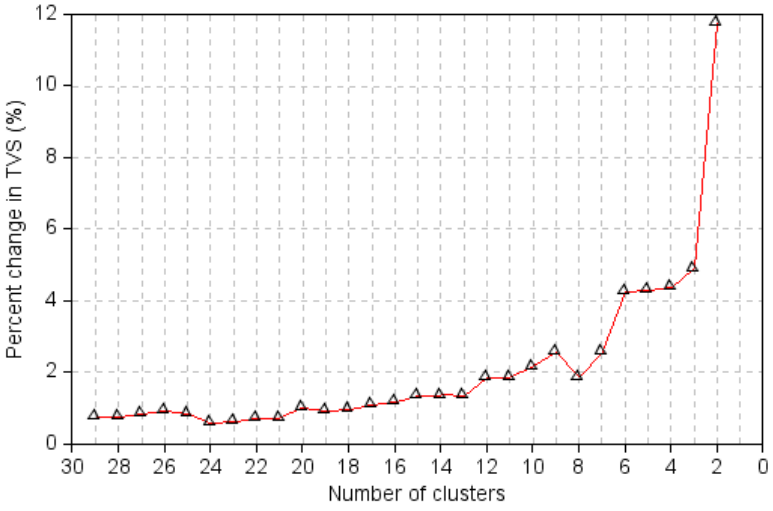

Figure 4.14. Number of Cluster graph in Erdemli in Spring in 1500 m height

The percentages of the wind for 9 clusters and the transportation routes to the station are shown in Figure 4.15. The spring profile is like the annual profile, but the profile from the southwest shows the dust transport more clearly. This profile has the 3rd highest percentage with %14.9 and reaches the region directly from the dust region of Libya and Egypt.

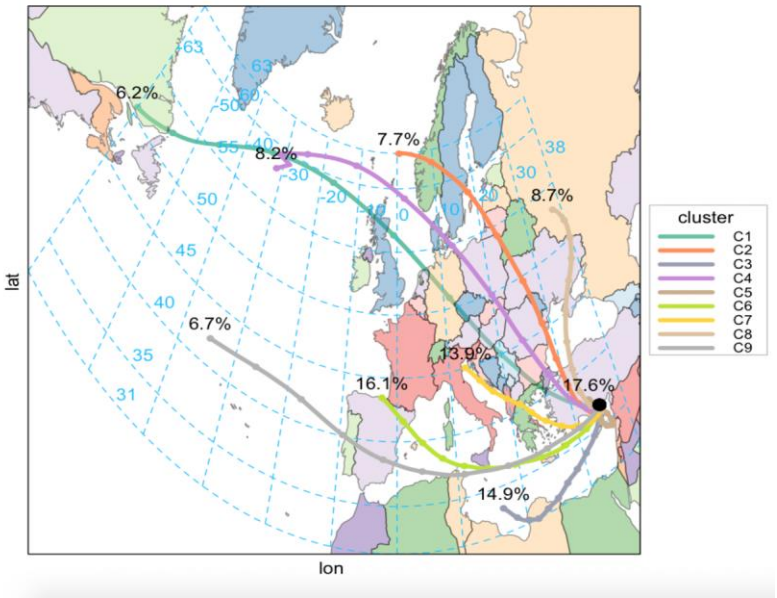

Figure 4.15. Cluster Analysis in Erdemli in Spring in 1500 m height

Graphics of the Summer season are given between Figure 4.16 and Figure 4.18. AOTs between 0.15 and 0.4 have 30-80% fine mode number density contribution between 0.05-0.15 μm radii, as seen in Figure 4.16. Fresh smoke aerosols are observed in areas where Ǽ is negative, the fine mode fraction is above 70%, and the AE is greater than 1.5. The remaining areas are associated with urban aerosols.

In cases where AOTs are greater than 0.4, it can be said that in areas with positive Ǽ, the coarse mode is effective alone, and where Ǽ is negative, the coarse mode is effective together with the fine mode. 0.15 μm radius line demonstrates the presence of biomass-burning aerosols with increasing fine mode fraction and AE.

AOTs greater than 0.7 are seen between the radius of 0.15-0.2 μm with 90% coarse mode number density contribution in the area where AE is less than 0.5. AOTs in this section show dust transport; the highest AOT observed was 1.5. Dust transport is also seen in the Summer, but in the Spring, it is relatively higher.

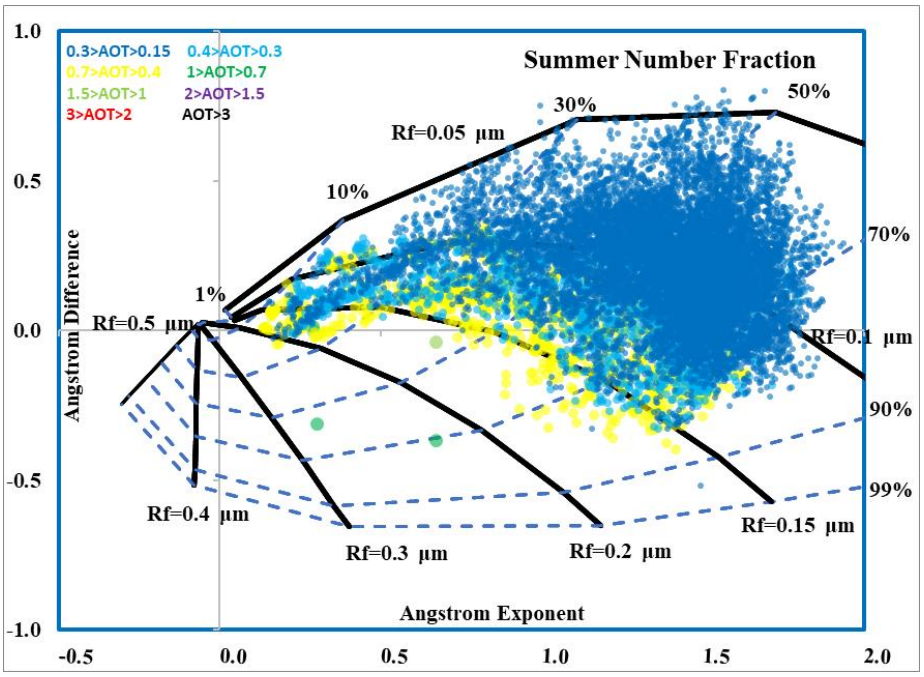

Figure 4.16. Seasonal aerosol classification by number fraction of fine mode-Summer

Figure 4.17 shows a shift in the area associated with dust transport at AOTs between 0.4 and 0.7. In this area, the contribution of the coarse mode to the total volume is calculated between approximately 90% and 98%. The contribution of fine mode to volume ratios is evaluated, and it is found that volume ratios increase up to 50%. It has been observed that dust is quite effective in the region in this season as well.

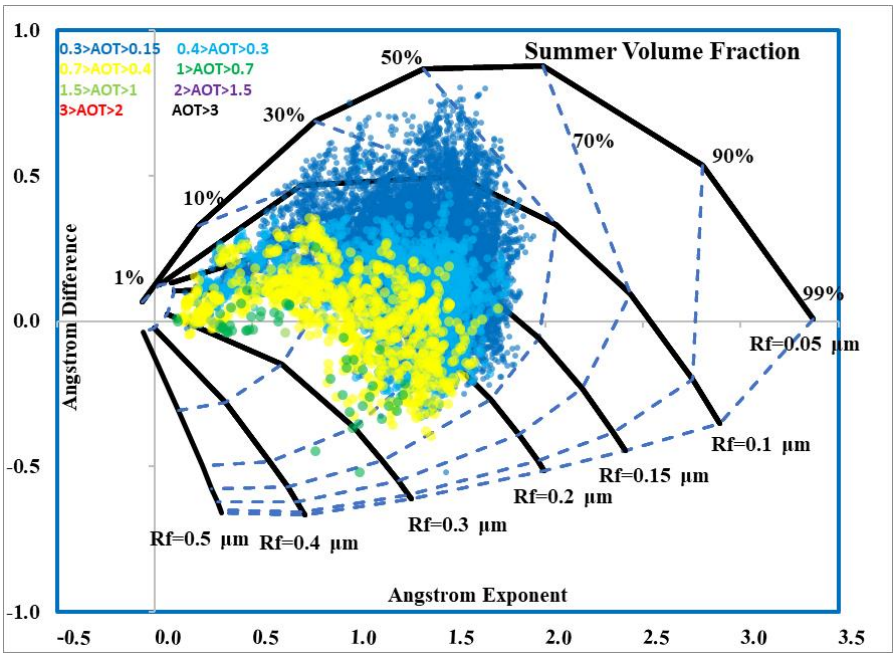

Figure 4.17. Seasonal aerosol classification by volume fraction of fine mode - Summer

Figure 4.18 shows that the coarse mode volume ratio decreases slightly at AOTs between 0.4 and 0.7. The accumulation mode is also likely effective in the dust particles transported to the region for this season.

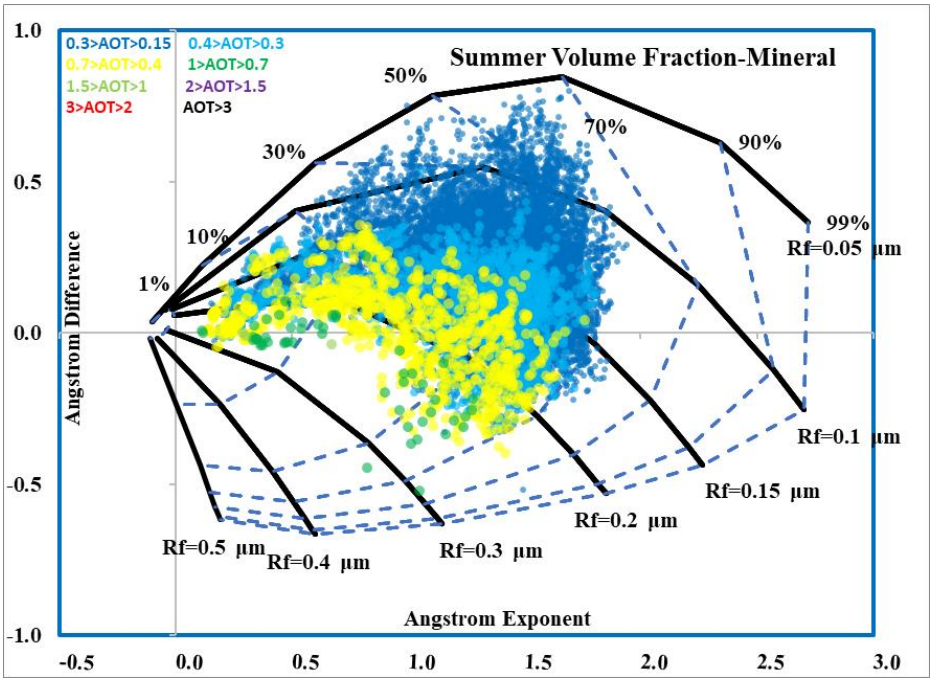

Figure 4.18. Seasonal aerosol classification by volume fraction of fine mode- Summer, mineral transported model

Before the general wind profiles for the region of Summer at 1500 m height were drawn, the required number of clusters was determined with the help of the graphic shown in

Figure 4.19. In the profile to be created for the selected 11 years, the number of clusters is calculated as 7.

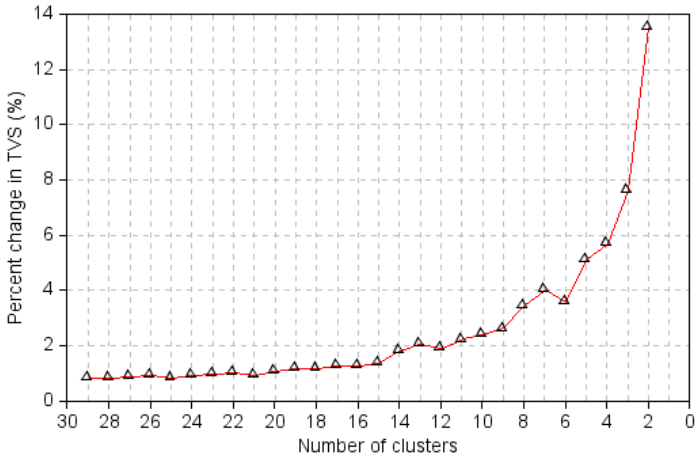

Figure 4.19. Number of Cluster graph in Erdemli in Summer in 1500 m height

The percentages of the wind for 7 clusters and the transportation routes to the station are shown in Figure 4.20. The summer profile follows the annual profile, with the highest profile from northern regions. Aerosol transport occurs both from the countries in the northern region and from Europe to the region. As in the annual profile, the ocean winds increase the region's sea salt aerosol load. Cluster 5, with 16% from the southwest, causes dust transport to the region.

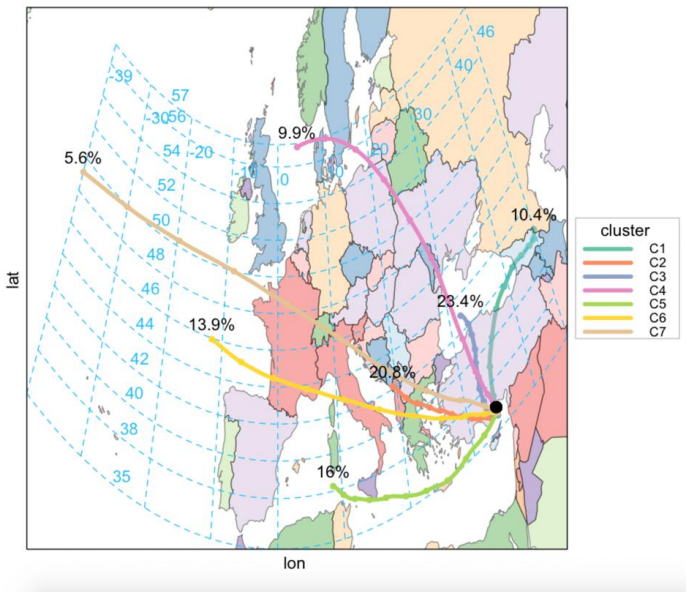

Figure 4.20. Cluster Analysis in Erdemli in Summer in 1500 m height

Graphics of the Autumn season are given between Figure 4.21 and Figure 4.23. AOTs of Autumn are evaluated, as seen in Figure 4.21, based on the number density fraction, and

it is found that the highest value rises to 1. AOTs between 0.15 and 0.3 are seen between 0.05 and 0.12 μm radii with a 30-70% fine mode number density contribution. The part where AE is less than 0.3 and AOT values between 0.4 and 1 with positive Ǽ are seen, and the contribution of fine mode to the total is between 10-30%, indicating the presence of dust. As in other seasons, fresh smoke, biomass-burning, and urban aerosols are seen in Autumn, and the size of dust-borne aerosols is observed to be smaller.

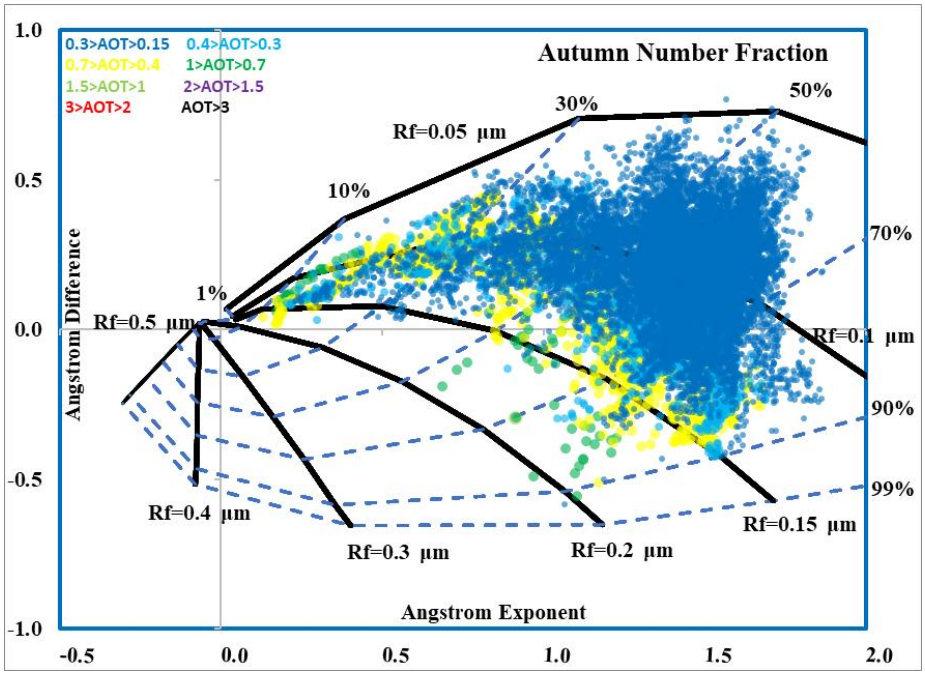

Figure 4.21. Seasonal aerosol classification by number fraction of fine mode- Autumn

Considering the volume ratios in Figure 4.27, coarse mode contribution to AOT greater than 0.4 is between 70-99%. The coarse mode number density for the same condition is between 30-99%. As can be seen, when the volume is considered, the effect of the coarse mode is seen more clearly.

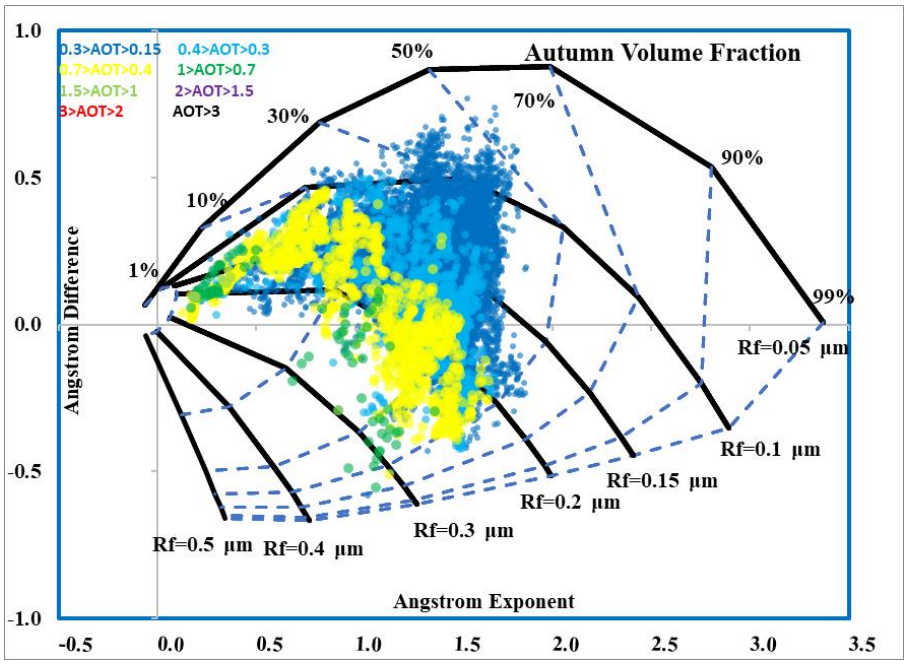

Figure 4.22. Seasonal aerosol classification by volume fraction of fine mode- Autumn

In Figure 4.23 that used for coarse mode dust transport, it is seen that the coarse mode volume slightly decreases with the area where AOTs is greater than 0.4.

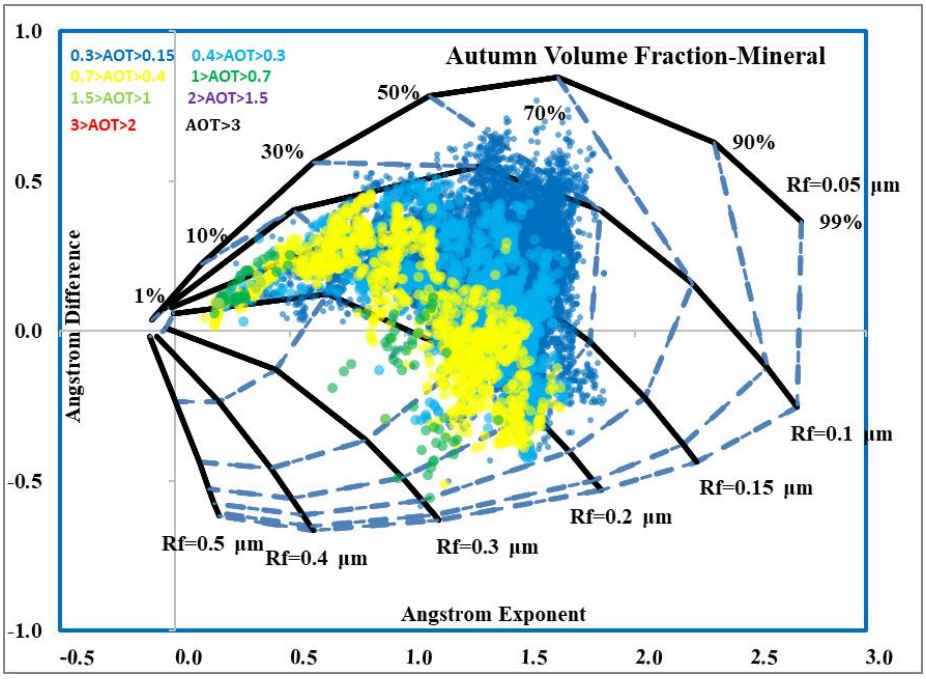

Figure 4.23. Seasonal aerosol classification by volume fraction of fine mode- Autumn, mineral transported model

Before the general wind profiles for the region of Autumn at 1500 m height were drawn, the required number of clusters was determined with the help of the graphic shown in

Figure 4.24. In the profile to be created for the selected 11 years, the number of clusters is calculated as 12.

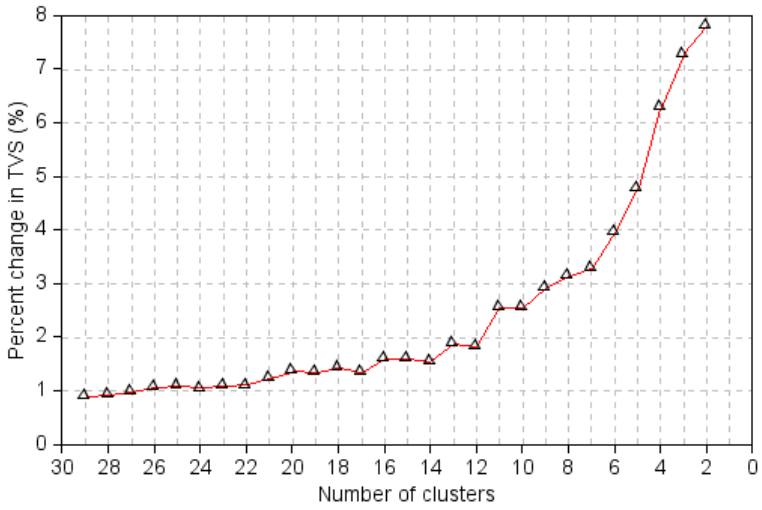

Figure 4.24. Number of Cluster graphs in Erdemli in Autumn in 1500 m height

The percentages of the wind for 12 clusters and the transportation routes to the station are shown in Figure 4.30. The autumn profile differs from the annual, spring, and summer profiles and has a higher number of clusters, and the amount of wind from the northwest over the ocean is negligible. With the decrease in the amount of wind coming from the ocean, aerosol aging was observed less in this season compared to the others. Although the regions with the highest winds are in the north and northwest, aerosol transport occurs with the winds coming from the countries around the region. In this season, dust transport occurs with a wind amount of 7.3% from the southwest.

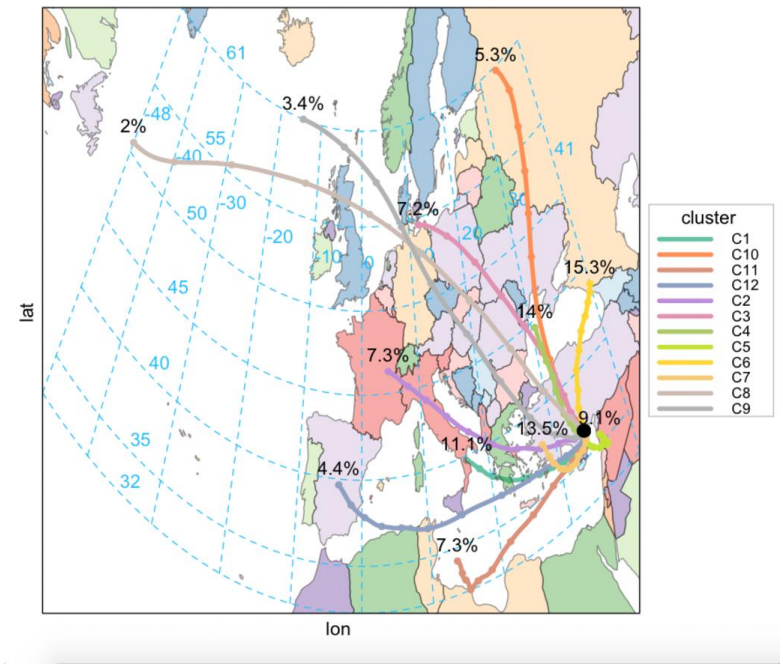

Figure 4.25. Cluster Analysis in Erdemli in Autumn in 1500 m height

Graphics of the Winter season are given between Figure 4.26 and Figure 4.28. The AOTs of this season are examined in Figure 4.26 based on number density fraction and seen that the AOT is one at most. AOTs between 0.15 and 0.4 are seen in the range of radii of 0.07 and 0.15 μm. As in other seasons, the fine mode number contribution is between 30% and 90%. The part where AE is less than 0.3 and AOT between 0.4 and 1 with positive Æ are seen, and the contribution of fine mode to the total is between 10-20%, indicating the presence of dust. As in other seasons, fresh smoke, biomass-burning, and urban aerosols are seen in winter, and the size of dust-borne aerosols is observed to be smaller.

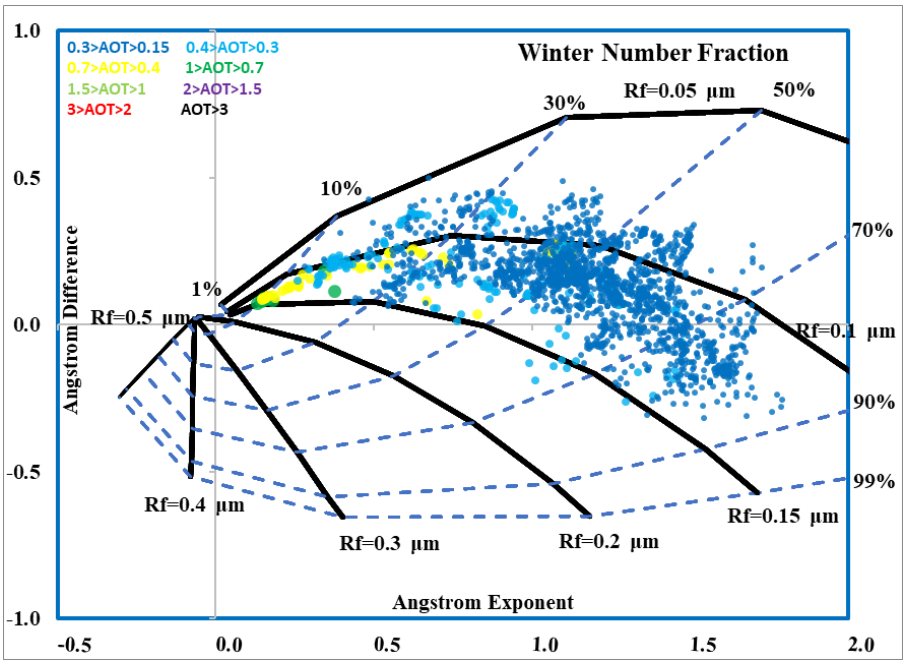

Figure 4.26. Seasonal aerosol classification by number fraction of fine mode- Winter

Considering the volume ratios in Figure 4.27, coarse mode contribution to AOTs greater than 0.4 is between 90-99%. The coarse mode number density for the same condition is between 70-90%. As can be seen, when the volume is taken into account, the effect of the coarse mode is seen more clearly.

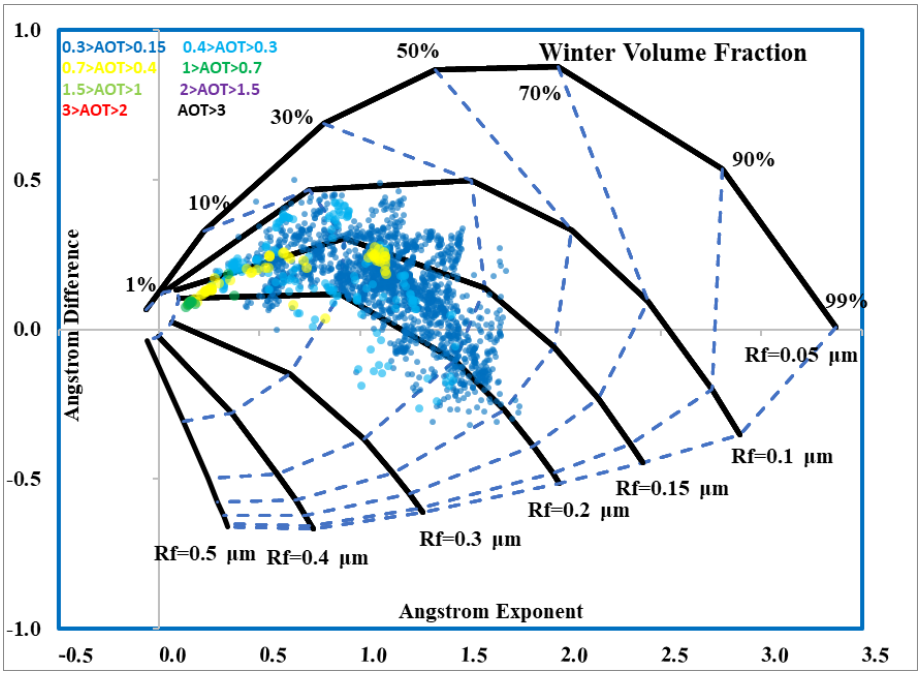

Figure 4.27. Seasonal aerosol classification by volume fraction of fine mode- Winter

In Figure 4.28, used for coarse mode dust transport, it is seen that the coarse mode volume slightly decreases with the area where the AOT is greater than 0.4.

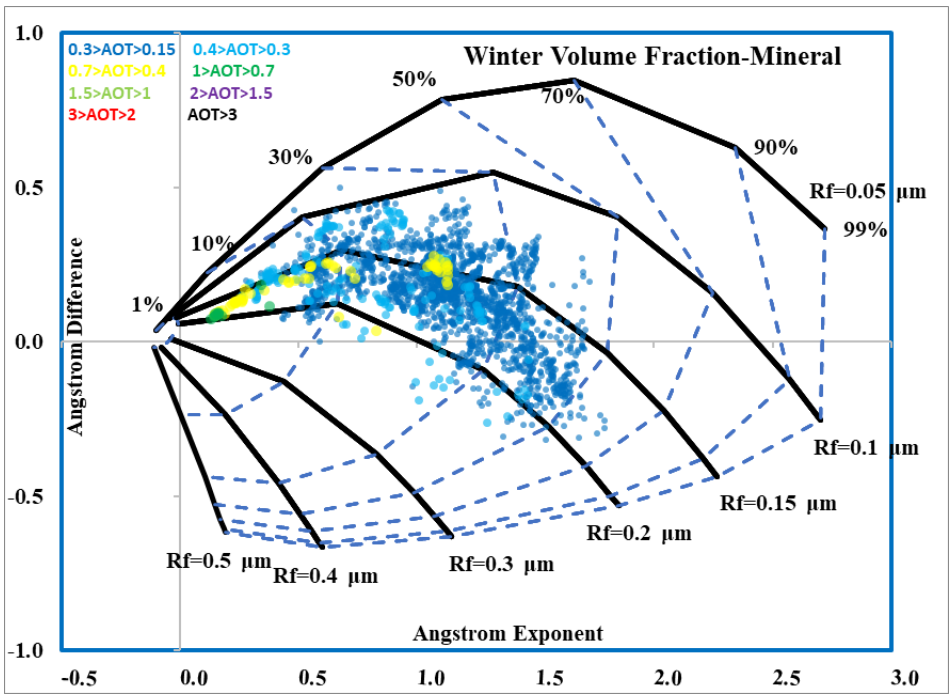

Figure 4.28. Seasonal aerosol classification by volume fraction of fine mode- Winter, mineral transported model

Before the general wind profiles for the region of Winter at 1500 m height were drawn, the required number of clusters was determined with the help of the graphic shown in Figure 4.29. In the profile to be created for the selected 11 years, the number of clusters is calculated as 7.

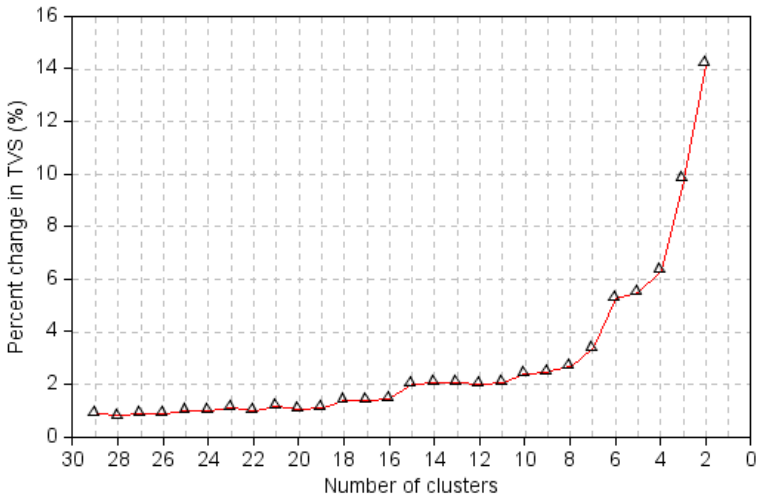

Figure 4.29. Number of Cluster graphs in Erdemli in Winter in 1500 m height

The percentages of the wind for 7 clusters and the transportation routes to the station are shown in Figure 4.30. The winter profile follows the annual profile, with the wind coming from the highest northern regions. Aerosol transport occurs both from the countries in the northern region and from Europe to the region. As in the annual profile, the ocean winds increase the region's aerosol load. 14.7% of wind from the southwest causes dust transport to the region.

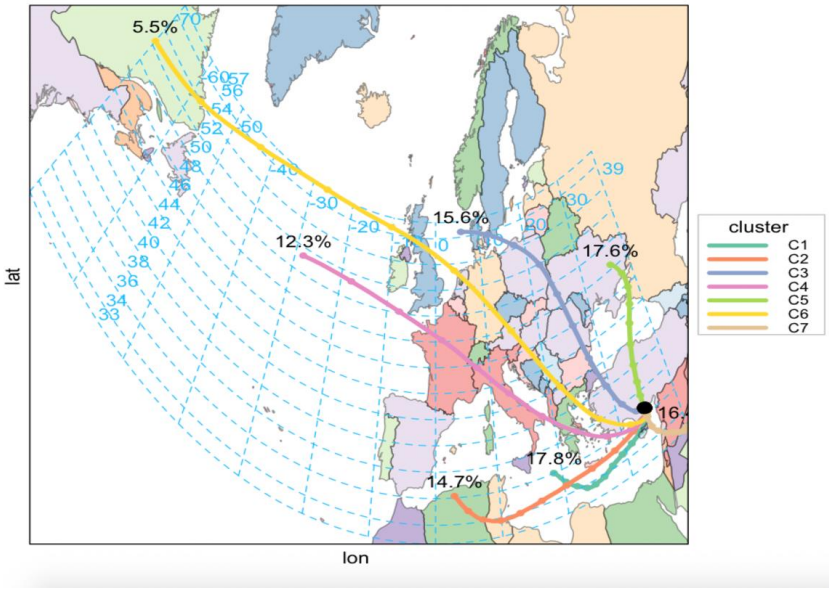

Figure 4.30. Cluster Analysis in Erdemli in Winter in 1500 m height

According to the analysis results, the season in which the dust is most intense is Spring. Intense dust transport was also observed in the Summer. While dust transport in summer increases AOT values up to 1.5, this value increases to 2.8 in Spring. As a result of the classifications made, it was determined that the dust was also transported to the region in the accumulation mode. According to the wind profiles, it was determined that dust was carried to the region from the southwest throughout the year. In Spring, winds come more from the region mentioned above is less than in summer. However, dust-induced AOT growth in the area is higher in Spring. In light of this information, it is thought that the dust transported to the region in summer is dense in accumulation mode. In autumn, there was a significant decrease in the amount of wind coming over the ocean. Accordingly, less aerosol hydration was observed in autumn compared to other seasons.

4.2.1. Monthly Analysis

The data were categorized monthly are visualized between Figure 4.31 and Figure 4.42, and the graph created for the dust transported coarse mode refractive index was used in

the analysis. The highest dust transport was determined in April, March, and May. The highest AOTs were measured in April, and these AOTs have 0 and close to 0 AE values, taking place in the areas where the fine mode was the lowest. Therefore, the growth in the measured AOT values was caused by dust. In these three months, the volume contribution of the coarse mode is slightly higher in March compared to other months, while the AOT measured in April is the highest. While the lowest dust is seen in November, December, and January, the dust increases in February. According to the dust transport density, the months can be ordered as April, March, May, August, September, June, July, February, October, December, November, and January.

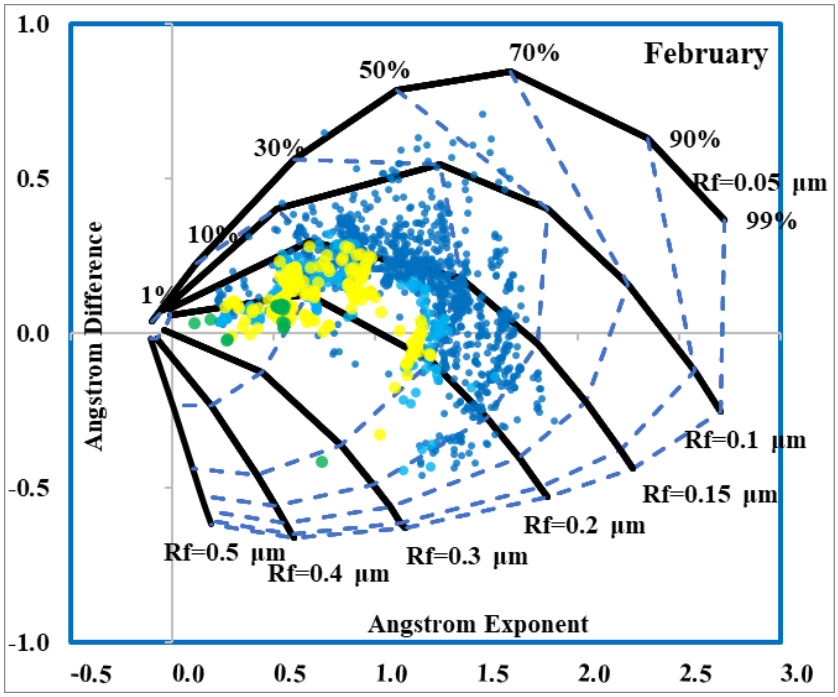

Figure 4.31. Monthly aerosol classification by volume fraction of fine mode, mineral transported model, February

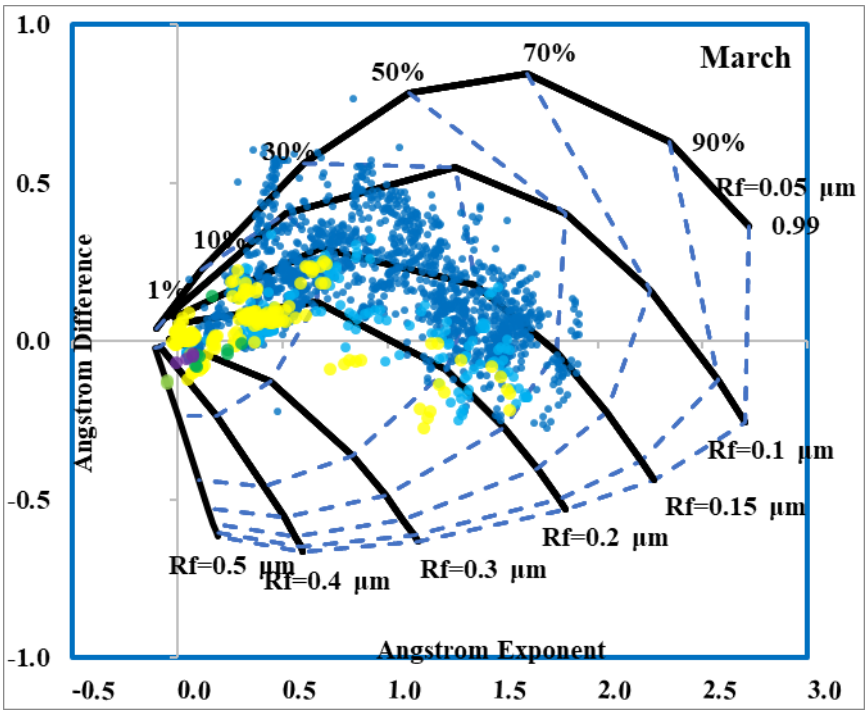

Figure 4.32. Monthly aerosol classification by volume fraction of fine mode, mineral transported model, March

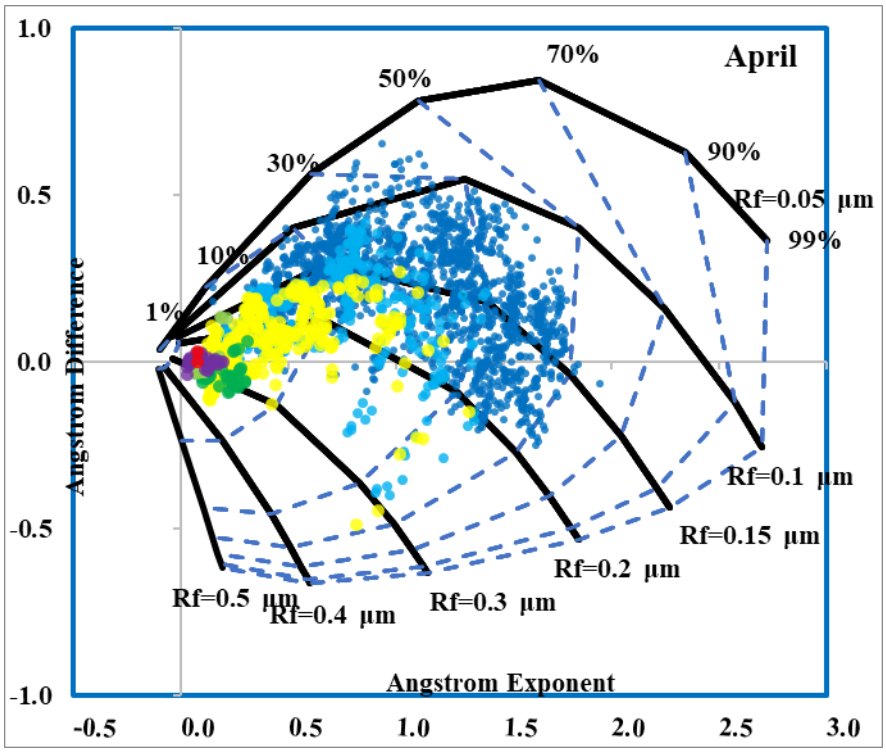

Figure 4.33. Monthly aerosol classification by volume fraction of fine mode, mineral transported model, April

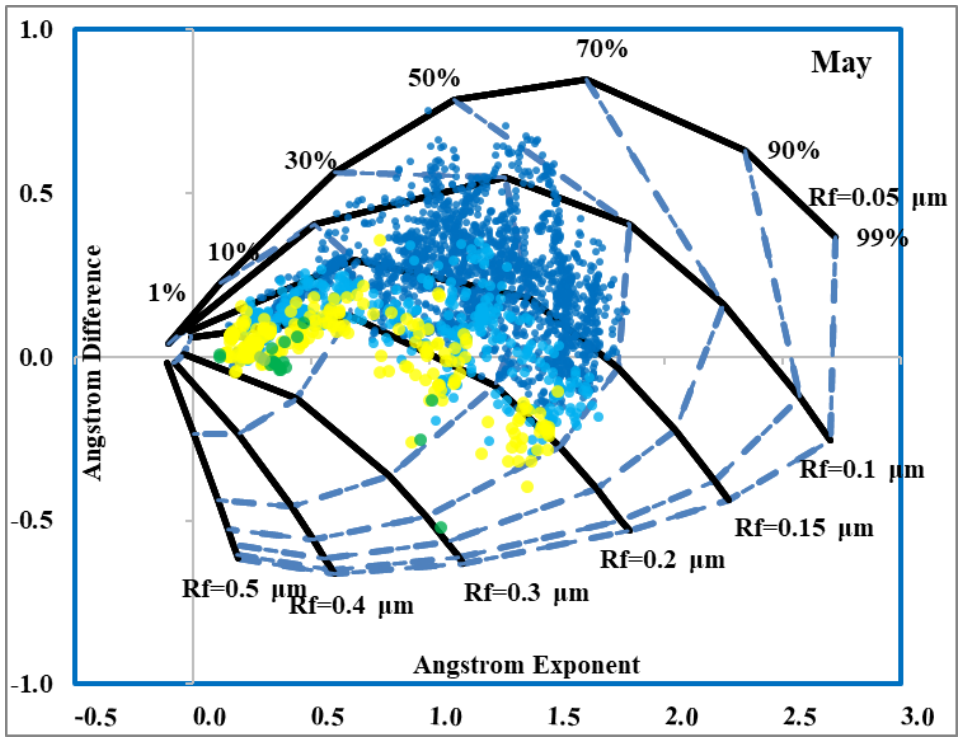

Figure 4.34. Monthly aerosol classification by volume fraction of fine mode, mineral transported model, May

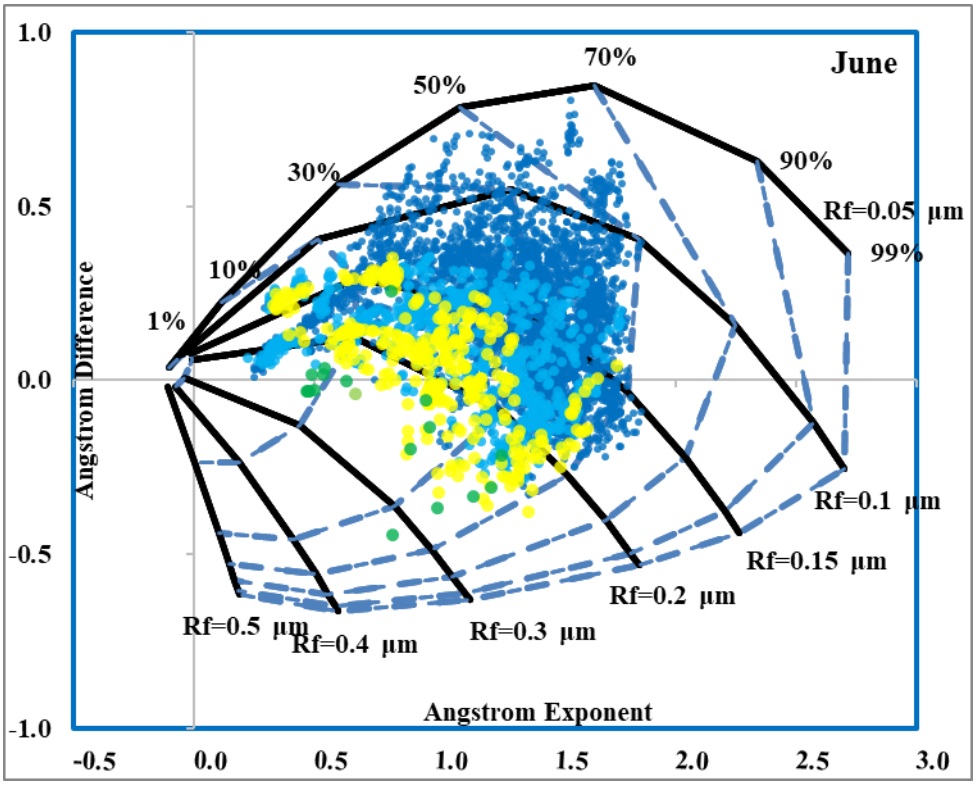

Figure 4.35. Monthly aerosol classification by volume fraction of fine mode, mineral transported model, June

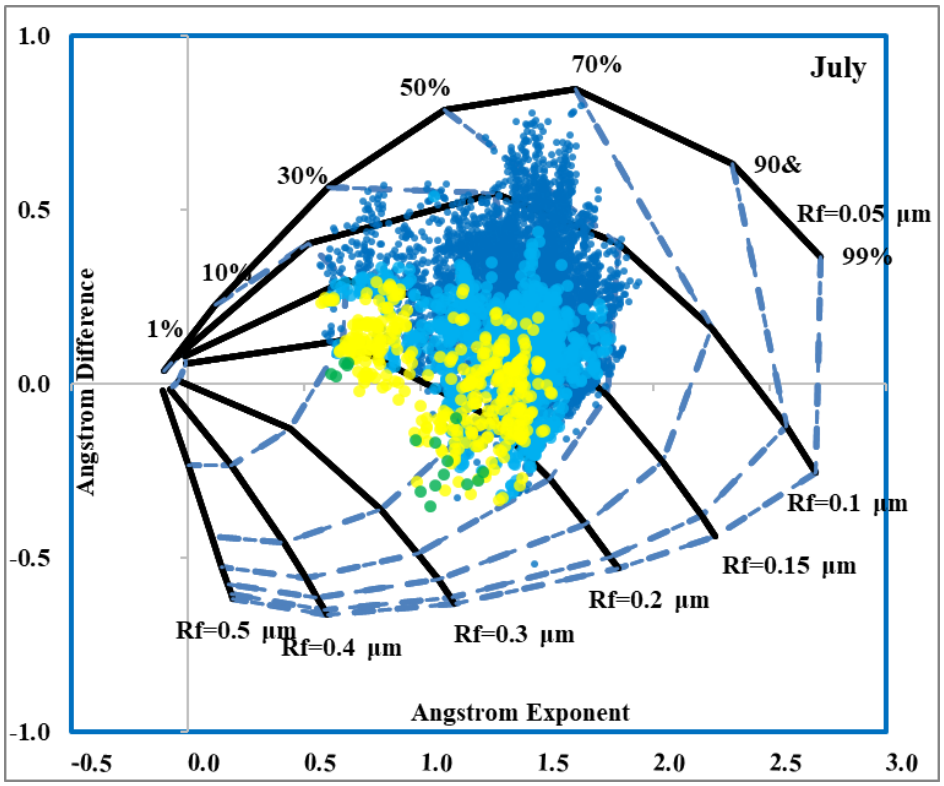

Figure 4.36. Monthly aerosol classification by volume fraction of fine mode, mineral transported model, July

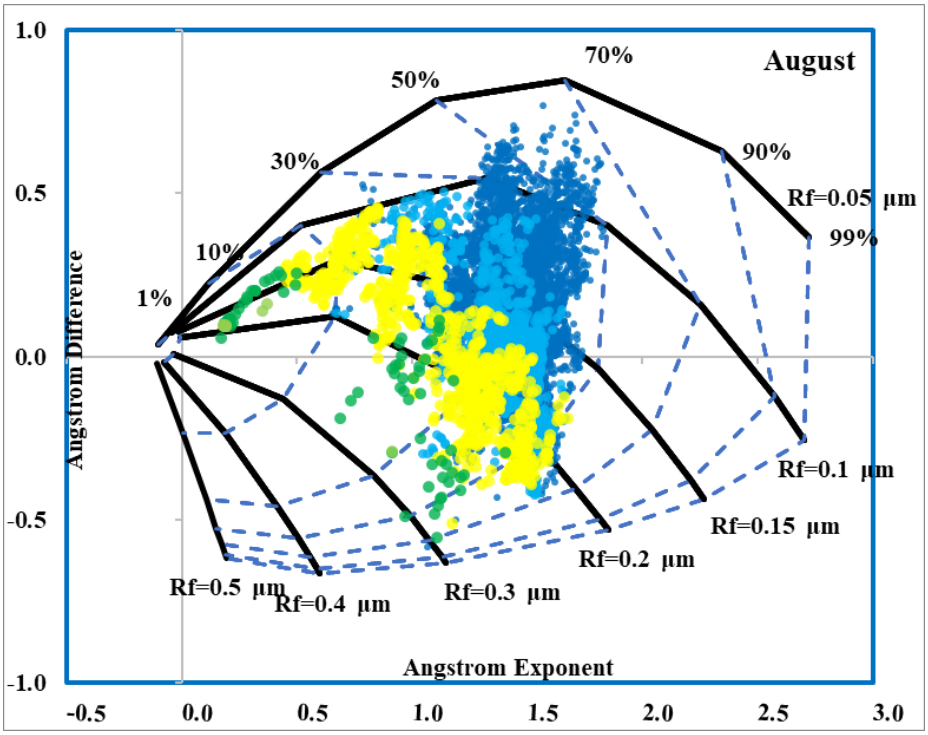

Figure 4.37. Monthly aerosol classification by volume fraction of fine mode, mineral transported model, August

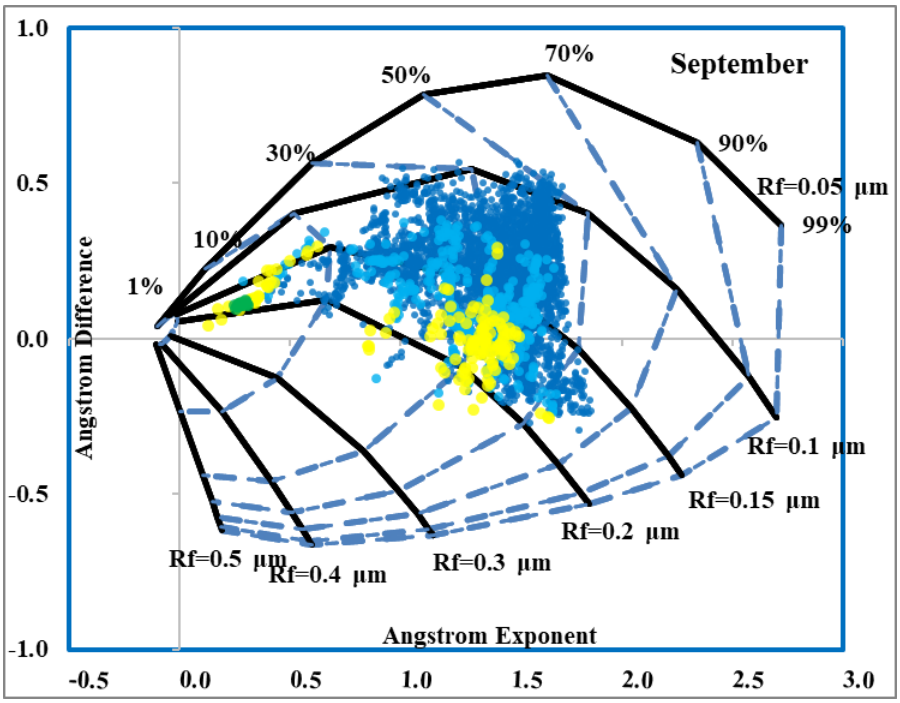

Figure 4.38. Monthly aerosol classification by volume fraction of fine mode, mineral transported model, September

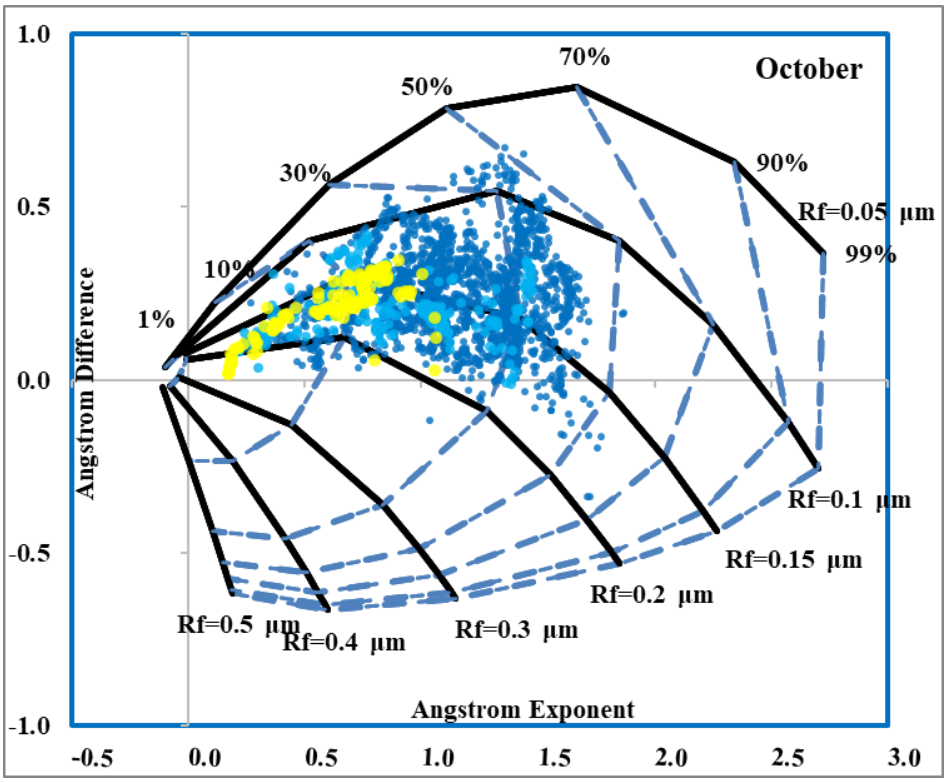

Figure 4.39. Monthly aerosol classification by volume fraction of fine mode, mineral transported model, October

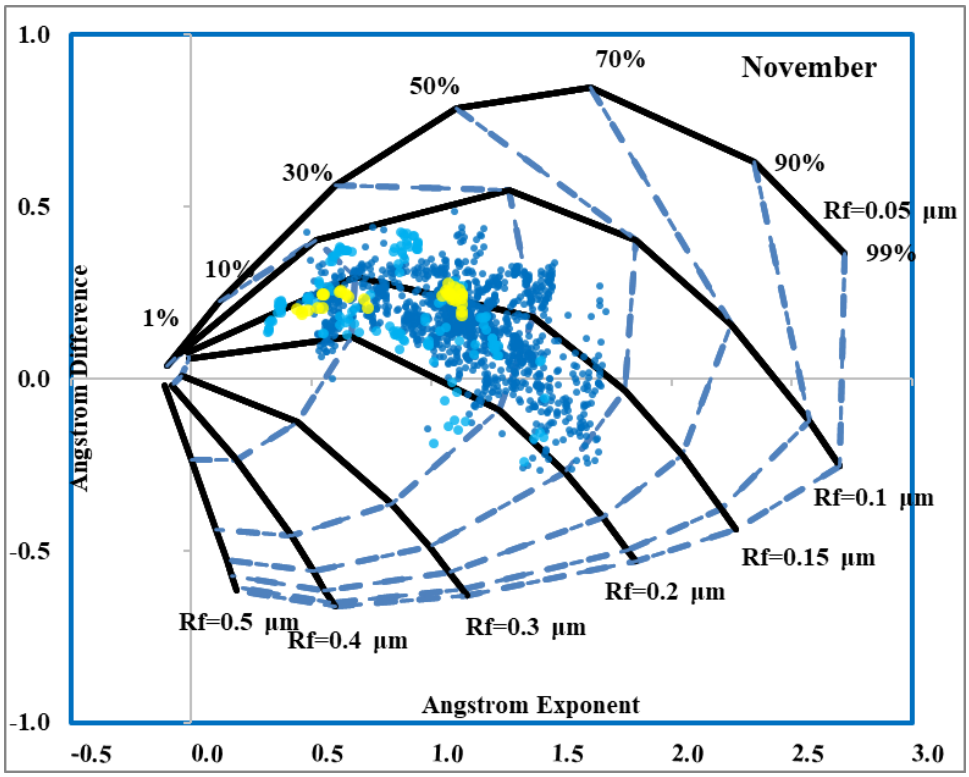

Figure 4.40. Monthly aerosol classification by volume fraction of fine mode, mineral transported model, November

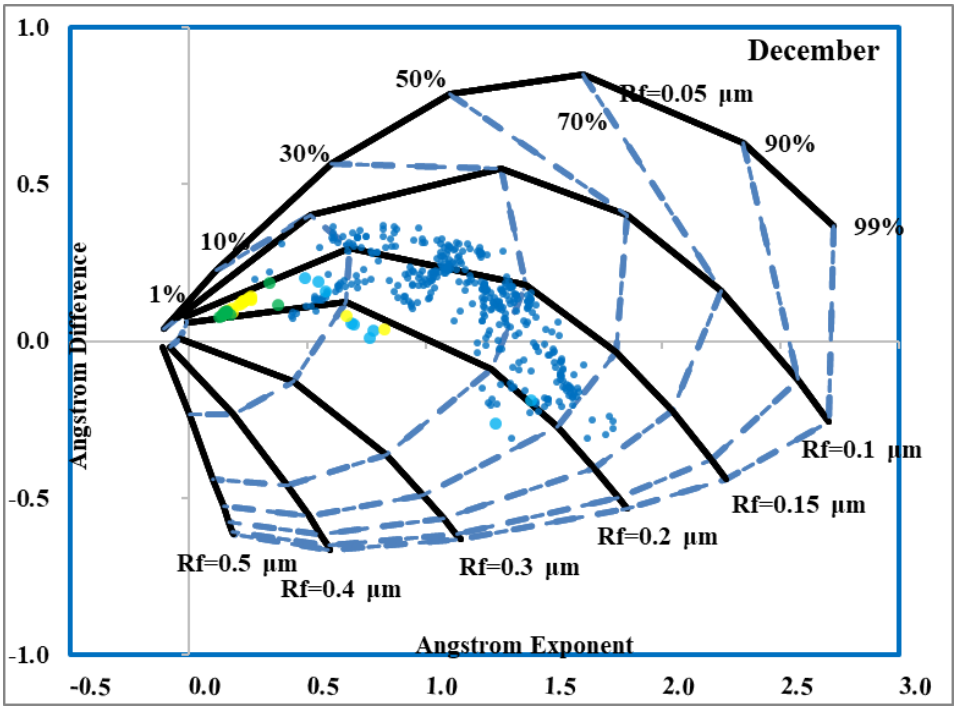

Figure 4.41. Monthly aerosol classification by volume fraction of fine mode, mineral transported model, December

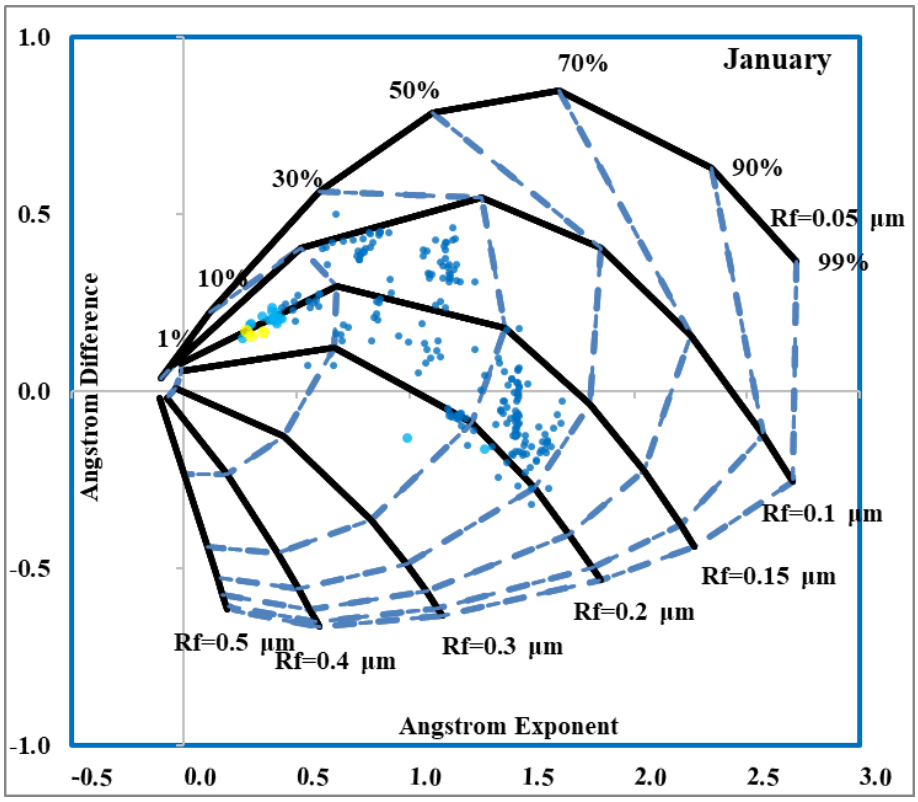

Figure 4.42. Monthly aerosol classification by volume fraction of fine mode, mineral transported model, January

5. CONCLUSION AND FUTURE WORK

According to annual analyzes, different aerosol types are detected in the region. Throughout the year, smoke, biomass burning, dust, and urban aerosols have been seen in the area. The number and volume ratios of fine mode to total load were evaluated for these aerosols in the periods in which they were effective. In addition, it has been observed that aerosols are effective in aging and hydration from time to time in the region. The presence of dust increases the volume effect of the large mode from 95% to 99%. In terms of volume, a large part of the aerosols of the region originates from the dust carried, and it constitutes the essential part of the aerosol load of the region. Even though the number density of the fine mode reaches 99%, the volume fractions get 50% at the most. Considering these data, the effect of the coarse mode resulting from dust transport is more important in the region.

As a result of the examinations made by separating the seasons, it is seen that there is dust transport to the region throughout the year, and it has been determined that the highest transport occurs in the spring. This season is followed by Summer, Autumn, and Winter; while AOT increases to 3 in Spring due to dust transport, this value increases to 1.5 in Summer and 1 in Autumn and Winter. The coarse mode number density fraction in the dust case is between 85-99% for spring, 85-90% for summer, and 70-90% for autumn and winter. The coarse mode volume density is 95-99% for spring and 90-93% for other seasons in the dust transport period.

According to the dust transport density on monthly analysis, the order from the highest dust transport to the lowest is as follows: April, March, May, August, September, June, July, February, October, December, November, and February.

The wind profiles of the region obtained according to 11-year data are evaluated, and it is found that the highest percentage is the wind profile coming from the southwest, followed by the profile from the northeast. The wind from the southwest is thought to be effective in dust transport to the region. Additionally, some of the winds in the region come from the ocean. There is urban aerosol transport along with the winds from Europe to the region. The seasonal wind profiles of the region show that in spring when the dust is at its highest throughout the year, the profile from the dust region of Libya and Egypt shows the dust transport clearly with a %14.9.

In all seasons, dust transport is clearly from the southwest, and in seasons except autumn, the effect of winds coming from the ocean to the region is seen. The autumn profile differs from the others and has a higher number of clusters, and the amount of wind from the northwest over the ocean is negligible. Wind from industrial and terrestrial regions causes an increase in the aerosol load of biomass burning and urban aerosols for all seasons.

As a summary of this study, it has been observed that dust is transported to the region throughout the year from the southwest and that most of the coarse-mode aerosols in the area are caused by dust transport. It was determined that dust transport was the region's most significant share in the increase of aerosol load, and the highest transport was observed in the spring months.

For further evaluations, sun photometers were installed in two regions of Turkey, and measurements were started. One selected region is Marmaris/Muğla, and the other is Diyarbakır. The Marmaris region was chosen to represent the southwest, and the Diyarbakir region represented the southeast. In future studies, classification will be carried out using the data obtained from these two newly established stations. The classification results of two new stations will be compared with the results of the Erdemli station, which is the subject of this thesis. As a result of the comparison, dust transport to the southern regions of Turkey will be evaluated, and dust transport routes will be examined for three different regions.

REFERENCES

Andrews, D. G. (2010). *An Introduction to Atmospheric Physics* (2nd ed.). Cambridge University Press. https://doi.org/DOI: 10.1017/CBO9780511800788

Aslanoğlu, S. Y., Proestakis, E., Gkikas, A., Güllü, G., & Amiridis, V. (2022). Dust Climatology of Turkey as a Part of the Eastern Mediterranean Basin via 9-Year CALIPSO-Derived Product. *Atmosphere*, *13*(5). https://doi.org/10.3390/atmos13050733

Atkinson, R. W., Bremner, S. A., Anderson, H. R., Strachan, D. P., Bland, J. M., & de Leon, A. P. (1999). Short-term associations between emergency hospital admissions for respiratory and cardiovascular disease and outdoor air pollution in London. *Archives of Environmental Health*, *54*(6), 398–411. https://doi.org/10.1080/00039899909603371

Basart, S., Pérez, C., Cuevas, E., Baldasano, J. M., & Gobbi, G. P. (2009). Aerosol characterization in Northern Africa, Northeastern Atlantic, Mediterranean Basin and Middle East from direct-sun AERONET observations. *Atmospheric Chemistry and Physics*, *9*(21), 8265–8282. https://doi.org/10.5194/acp-9-8265-2009

Brooks, D. (2008). Instrument Design Principles II: Sun Photometers. In *Bringing the Sun Down to Earth: Designing Inexpensive Instruments for Monitoring the Atmosphere* (pp. 28–29). Springer Netherlands. https://doi.org/10.1007/978-1-4020-8694-6_5

Calvo, A. I., Alves, C., Castro, A., Pont, V., Vicente, A. M., & Fraile, R. (2013). Research on aerosol sources and chemical composition: Past, current and emerging issues. *ATMOSPHERIC RESEARCH*, *120*, 1–28. https://doi.org/10.1016/j.atmosres.2012.09.021

CE318-T - Sun Sky Lunar Multispectral Photometer | Cimel Electronique. (n.d.). Retrieved November 25, 2022, from https://www.cimel.fr/solutions/ce318-t/

Chen, J., Li, C., Ristovski, Z., Milic, A., Gu, Y., Islam, M. S., Wang, S., Hao, J., Zhang, H., He, C., Guo, H., Fu, H., Miljevic, B., Morawska, L., Thai, P., LAM, Y. F., Pereira, G., Ding, A., Huang, X., & Dumka, U. C. (2017). A review of biomass burning: Emissions and impacts on air quality, health and climate in China. *Science of The Total Environment*, *579*, 1000–1034.

https://doi.org/https://doi.org/10.1016/j.scitotenv.2016.11.025

Cox, P. A. (2005). Diverse taxa of cyanobacteria produce β-N-methylamino-l-alanine, a neurotoxic amino acid. *Proc. Natl. Acad. Sci. U. S. A.*, *102*(14), 5074.

Davies, C. N. (1974). Size distribution of atmospheric particles. *Journal of Aerosol Science*, *5*(3), 293–300. https://doi.org/https://doi.org/10.1016/0021-8502(74)90063-9

Draxler, R., & Hess, G. (1998). An overview of the HYSPLIT_4 modeling system for trajectories. *Aust. Meteorol. Mag.*, *47*.

Eck, T. F., Holben, B. N., Reid, J. S., Dubovik, O., Smirnov, A., O'Neill, N. T., Slutsker, I., & Kinne, S. (1999). Wavelength dependence of the optical depth of biomass burning, urban, and desert dust aerosols. In *Journal of Geophysical Research Atmospheres* (Vol. 104, Issue D24, pp. 31333–31349). https://doi.org/10.1029/1999JD900923

Giles, D. M., Sinyuk, A., Sorokin, M. G., Schafer, J. S., Smirnov, A., Slutsker, I., Eck, T. F., Holben, B. N., Lewis, J. R., Campbell, J. R., Welton, E. J., Korkin, S. V, & Lyapustin, A. I. (2019). Advancements in the Aerosol Robotic Network (AERONET) Version~3 database -- automated near-real-time quality control algorithm with improved cloud screening for Sun photometer aerosol optical depth (AOD) measurements. *Atmospheric Measurement Techniques*, *12*(1), 169–209. https://doi.org/10.5194/amt-12-169-2019

Gobbi, G. P., Kaufman, Y. J., Koren, I., & Eck, T. F. (2007). Classification of aerosol properties derived from AERONET direct sun data. *Atmospheric Chemistry and Physics*, *7*(2), 453–458. https://doi.org/10.5194/acp-7-453-2007

Holben, B. N., Eck, T. F., Slutsker, I., Tanré, D., Buis, J. P., Setzer, A., Vermote, E., Reagan, J. A., Kaufman, Y. J., Nakajima, T., Lavenu, F., Jankowiak, I., & Smirnov, A. (1998). AERONET - A federated instrument network and data archive for aerosol characterization. *Remote Sensing of Environment*, *66*(1), 1–16. https://doi.org/10.1016/S0034-4257(98)00031-5

Junge, C. (1955). The Size Distribution and Aging of Natural Aerosols As Determined From Electrical and Optical Data on the Atmosphere. In *Journal of Meteorology* (Vol. 12, Issue 1, pp. 13–25). https://doi.org/10.1175/1520-

0469(1955)012<0013:tsdaao>2.0.co;2

Kaskaoutis, D. G., Kambezidis, H. D., Hatzianastassiou, N., Kosmopoulos, P. G., & Badarinath, K. V. S. (2007). Aerosol climatology: dependence of the Angstrom exponent on wavelength over four AERONET sites. *Atmospheric Chemistry and Physics Discussions*, *7*, 7347–7397. https://doi.org/10.5194/acpd-7-7347-2007

Kaufman, Y. J. (1993). Aerosol optical thickness and atmospheric path radiance. *Journal of Geophysical Research*, *98*(D2), 2677–2692. https://doi.org/10.1029/92JD02427

Kennedy, I. M. (2007). The health effects of combustion-generated aerosols. *Proceedings of the Combustion Institute*, *31 II*, 2757–2770. https://doi.org/10.1016/j.proci.2006.08.116

Kokhanovsky, A. A. (2008). Optical properties of atmospheric aerosol. In *Aerosol Optics: Light Absorption and Scattering by Particles in the Atmosphere* (pp. 16–47). Springer Berlin Heidelberg. https://doi.org/10.1007/978-3-540-49909-1_2

Kommalapati, R. R., & Valsaraj, K. T. (2009). Atmospheric aerosols and their importance. *ACS Symposium Series*, *1005*(5), 1–10. https://doi.org/10.1021/bk-2009-1005.ch001

Kuniyal, J. C., & Guleria, R. P. (2019). The current state of aerosol-radiation interactions: A mini review. *JOURNAL OF AEROSOL SCIENCE*, *130*, 45–54. https://doi.org/10.1016/j.jaerosci.2018.12.010

Lohmann, U. (2007). Aerosol Effects on Clouds and Climate. In Y. Calisesi, R.-M. Bonnet, L. Gray, J. Langen, & M. Lockwood (Eds.), *Solar Variability and Planetary Climates* (pp. 129–137). Springer New York. https://doi.org/10.1007/978-0-387-48341-2_10

Mauderly, J. L., & Chow, J. C. (2008). Health effects of organic aerosols. In *Inhalation Toxicology* (Vol. 20, Issue 3). https://doi.org/10.1080/08958370701866008

McMurry, P. H. (2000). A review of atmospheric aerosol measurements. *ATMOSPHERIC ENVIRONMENT*, *34*(12–14), 1959–1999. https://doi.org/10.1016/S1352-2310(99)00455-0

Mims, F. M. (1992). Sun photometer with light-emitting diodes as spectrally selective detectors. *Appl. Opt.*, *31*(33), 6965–6967. https://doi.org/10.1364/AO.31.006965

Morawska, L. (2003). Environmental aerosol physics. *Brisbane, Queensland University of Technology*, *38*(13), 1839–1850. http://linkinghub.elsevier.com/retrieve/pii/S1352231004000755%5Cnhttp://www.biophysics.sbg.ac.at/transcript/aerosol2.pdf

Morys, M., Mims III, F., Hagerup, S., Anderson, S., Baker, A., Kia, J., & Walkup, T. (2001). Design, calibration, and performance of MICROTOPS II handheld ozone monitor and Sun photometer. *J. Geophys. Res.*, *582*, 514–573. https://doi.org/10.1029/2001JD900103

Myhre, G., Lund Myhre, C., Samset, B. H., & Storelvmo, T. (2013). Aerosols and their Relation to Global Climate and Climate Sensitivity. *Nature Education Knowledge*, *4*, 7.

Payan, S., De La Noe, J., Hauchecorne, A., & Camy-Peyret, C. (2005). A review of remote sensing techniques and related spectroscopy problems. *COMPTES RENDUS PHYSIQUE*, *6*(8), 825–835. https://doi.org/10.1016/j.crhy.2005.07.013

Pöschl, U. (2005). Atmospheric Aerosols: Composition, Transformation, Climate and Health Effects. *Angewandte Chemie International Edition*, *44*(46), 7520–7540. https://doi.org/https://doi.org/10.1002/anie.200501122

Quirantes, A., Guerrero-Rascado, J. L., Pérez-Ramírez, D., Foyo-Moreno, I., Ortiz-Amezcua, P., Benavent-Oltra, J. A., Lyamani, H., Titos, G., Bravo-Aranda, J. A., Cazorla, A., Valenzuela, A., Casquero-Vera, J. A., Bedoya-Velásquez, A. E., Alados-Arboledas, L., & Olmo, F. J. (2019). Extinction-related Angström exponent characterization of submicrometric volume fraction in atmospheric aerosol particles. *Atmospheric Research*, *228*, 270–280. https://doi.org/https://doi.org/10.1016/j.atmosres.2019.06.009

Rap, A., Scott, C. E., Spracklen, D. V., Bellouin, N., Forster, P. M., Carslaw, K. S., Schmidt, A., & Mann, G. (2013). Natural aerosol direct and indirect radiative effects. *Geophysical Research Letters*, *40*(12), 3297–3301. https://doi.org/10.1002/grl.50441

Schuster, G. L., Dubovik, O., & Holben, B. N. (2006). Angstrom exponent and bimodal aerosol size distributions. *Journal of Geophysical Research Atmospheres*, *111*(7), 1–14. https://doi.org/10.1029/2005JD006328

Shifrin, K. S. (1995). Simple relationships for the Ångström parameter of disperse systems. *Appl. Opt.*, *34*(21), 4480–4485. https://doi.org/10.1364/AO.34.004480

Slanina, J. (2004). Air Pollution from Energy Production and Use. In C. J. Cleveland (Ed.), *Encyclopedia of Energy* (pp. 39–54). Elsevier. https://doi.org/https://doi.org/10.1016/B0-12-176480-X/00387-9

Verma, S., Prakash, D., Soni, M., & Ram, K. (2019). Atmospheric Aerosols Monitoring: Ground and Satellite-Based Instruments. In S. Sarvajayakesavalu (Ed.), *Advances in Environmental Monitoring and Assessment*. IntechOpen. https://doi.org/10.5772/intechopen.80489

Volz, F. (1959). Photometer mit Selen-Photoelement zur spektralen Messung der Sonnenstrahlung und zur Bestimmung der Wellenlängenabhängigkeit der Dunsttrübung. *Archiv Für Meteorologie, Geophysik Und Bioklimatologie, Serie B*, *10*(1), 100–131. https://doi.org/10.1007/BF02243122

Volz, F. E. (1974). Economical Multispectral Sun Photometer for Measurements of Aerosol Extinction from 0.44 μm to 1.6 μm and Precipitable Water. *Appl. Opt.*, *13*(8), 1732–1733. https://doi.org/10.1364/AO.13.001732

Whitby, K. T. (1978). The physical characteristics of sulfur aerosols. *Atmospheric Environment (1967)*, *12*(1), 135–159. https://doi.org/https://doi.org/10.1016/0004-6981(78)90196-8